Binding of the Proline-Rich Segment of Myelin Basic Protein to SH3 Domains: Spectroscopic, Microarray, and Modeling Studies of Ligand Conformation and Effects of Posttranslational Modifications†

Eugenia Polverini,‡ Godha Rangaraj,§ David S. Libich,|| Joan M. Boggs,§ and George Harauz*,||

Dipartimento di Fisica and CNISM, Università di Parma, V. le Usberti, 7/A, 43100 Parma, Italy, Department of Molecular Structure and Function, Research Institute, Hospital for Sick Children, 555 University Avenue, Toronto, Ontario M5G 1X8, Canada, Department of Laboratory Medicine and Pathobiology, University of Toronto, Toronto, Ontario M5G 1L5, Canada, and Department of Molecular and Cellular Biology, and Biophysics Interdepartmental Group, University of Guelph, 50 Stone Road East, Guelph, Ontario N1G 2W1, Canada

Received July 6, 2007; Revised Manuscript Received September 27, 2007

ABSTRACT: Myelin basic protein (MBP) is a multifunctional protein involved in maintaining the stability and integrity of the myelin sheath by a variety of interactions with membranes and with cytoskeletal and other proteins. A central segment of MBP is highly conserved in mammals and consists of a membrane surface-associated amphipathic α-helix, immediately followed by a proline-rich segment that we hypothesize is an SH3 ligand. We show by circular dichroic spectroscopy that this proline-rich segment forms a polyproline type II helix in vitro under physiological conditions and that phosphorylation at a constituent threonyl residue has a stabilizing effect on its conformation. Using SH3 domain microarrays, we observe that the unmodified recombinant murine 18.5 kDa MBP isoform (rmC1 component) binds the following SH3 domains: Yes1 > PSD95 > cortactin = PexD = Abl = Fyn = c-Src = Itk in order of decreasing affinity. A quasi-deiminated form of the protein (rmC8) binds the SH3 domains Yes1 > Fyn > cortactin = c-Src > PexD = Abl. Phosphorylation of rmC1 at 1−2 threonines within the proline-rich segment by mitogen-activated protein kinase in vitro has no effect on the binding specificity to the SH3 domains on the array. An SH3 domain of chicken Fyn is also demonstrated to bind to lipid membrane-associated C1, phosphorylated C1, and rmC8. Molecular docking simulations of the interaction of the putative SH3 ligand of classic MBP with the human Fyn SH3 domain indicate that the strength of the interaction is of the same order of magnitude as with calmodulin and that the molecular recognition and association is mediated by some weak CH···π interactions between the ligand prolyl residues and the aromatic ones of the SH3 binding site. One such interaction is well-conserved and involves the stacking of an MBP-peptide prolyl and an SH3 domain tryptophanyl residue, as in most other SH3−ligand complexes. Lysyl and arginyl residues in the peptide canonically interact via salt bridges and cation−π interactions with negatively charged and aromatic residues in the SH3 domain binding site. Posttranslational modifications (phosphorylation or methylation) of the ligand cause noticeable shifts in the conformation of the flexible peptide and its side chains but do not predict any major inhibition of the binding beyond somewhat less favorable interactions for peptides with phosphorylated seryl or threonyl residues.

The myelin basic protein (MBP)[1] family arises from the genetic unit called Golli (genes of the oligodendrocyte lineage) via use of several different transcription sites (tss1, tss2, and tss3), alternative splicing, and regulation by a combinatorial network of control sequences (*1*). The classic (from tss3) 18.5 kDa MBP isoform (Figure 1) is one of the major protein components of human and bovine central nervous system myelin (14 kDa in mice) and maintains the tight multilamellar packing of the sheath (*2*, *3*). The Golli-

† This work was supported by the Istituto Nazionale per la Fisica della Materia (INFM), the Canadian Institutes of Health Research (MOP 6506 to J.M.B. and MOP 74468 to G.H.), and the Natural Sciences and Engineering Research Council of Canada (Discovery Grant RG121541 to G.H.). D.S.L. was the recipient of an Ontario Graduate Scholarship.

* Author to whom correspondence should be addressed: phone 519-824-4120, ext. 52535; fax 519-837-1802; e-mail gharauz@uoguelph.ca.

‡ Università di Parma.

§ Hospital for Sick Children and University of Toronto.

|| University of Guelph.

[1] Abbreviations: ADM, asymmetrically dimethylated; ADT, AutoDockTools; bC1, bovine myelin basic protein charge isomer C1; ds, docking simulation; Golli, genes of the oligodendrocyte lineage; GSK-3β, glycogen synthase kinase 3β; GST, glutathione-S-transferase; HRP, horseradish peroxidase; MAGUK, membrane-associated guanylate kinase; MAP, microtubule-associated protein; MAPK, mitogen-activated protein kinase; MBP, myelin basic protein; MLV, multilamellar vesicle; MM, monomethylated; NRTK, nonreceptor tyrosine kinase; PC, phosphatidylcholine; PDB, Protein Data Bank; PG, phosphatidylglycerol; Ph-bC1, phosphorylated bC1; Ph-rmC1, phosphorylated rmC1; PLC, phospholipase C; PPII, polyproline type II; PhS, phosphorylated serine; PhT, phosphorylated threonine; PSD95, presynaptic density protein 95; rmC1, recombinant murine myelin basic protein C1 component; rmC8, recombinant murine myelin basic protein C8 component; RMSD, root mean square deviation; SDM, symmetrically dimethylated; SH3, Src homology domain 3; ZO-1, zonula occludens 1.

10.1021/bi701336n CCC: $40.75
Published on Web 12/08/2007

```
                        [exon-I.....................................
21.5  kDa mMBP       MASQKRPSQR SKYLATASTM DHARHGFLPR HRDTGILDSI GRFFSGDRGA
20.2  kDa mMBP       MASQKRPSQR SKYLATASTM DHARHGFLPR HRDTGILDSI GRFFSGDRGA
18.5  kDa mMBP    0> MASQKRPSQR SKYLATASTM DHARHGFLPR HRDTGILDSI GRFFSGDRGA
18.5  kDa rmC1    0> MASQKRPSQR SKYLATASTM DHARHGFLPR HRDTGILDSI GRFFSGDRGA
18.5  kDa rmC8    0> MASQKRPSQR SKYLATASTM DHAQHGFLPR HQDTGILDSI GRFFSGDRGA
17.24 kDa mMBP       MASQKRPSQR SKYLATASTM DHARHGFLPR HRDTGILDSI GRFFSGDRGA
17.22 kDa mMBP       MASQKRPSQR SKYLATASTM DHARHGFLPR HRDTGILDSI GRFFSGDRGA
14.0  kDa mMBP       MASQKRPSQR SKYLATASTM DHARHGFLPR HRDTGILDSI GRFFSGDRGA
                        [exon-I.....................................

                        exon-I][exon-II.............exon-II][exon-III.........
21.5  kDa mMBP       PKRGSGKVPW LKQSRSPLPS HARSRPGLCH MYKDSHTRTT HYGSLPQKSQ
20.2  kDa mMBP       PKRGSGKVPW LKQSRSPLPS HARSRPGLCH MYKDSHTRTT HYGSLPQKSQ
18.5  kDa mMBP  50> PKRGSGK                                DSHTRTT HYGSLPQKSQ
18.5  kDa rmC1  50> PKRGSGK                                DSHTRTT HYGSLPQKSQ
18.5  kDa rmC8  50> PKRGSGK                                DSHTRTT HYGSLPQKSQ
17.24 kDa mMBP       PKRGSGK                                DSHTRTT HYGSLPQKSQ
17.22 kDa mMBP       PKRGSGKVPW LKQSRSPLPS HARSRPGLCH MYKDSHTRTT HYGSLPQKSQ
14.0  kDa mMBP       PKRGSGK                                DSHTRTT HYGSLPQKSQ
                        exon-I][exon-II.............exon-II][exon-III.........

                        .........exon-III][exon-IV..IV][exon-V...V] [exon-VI..
21.5  kDa mMBP       HGRTQDENPV VHFFKNIVTP RTPPPSQGKG RGLSLSRFSW GAEGQKPGFG
20.2  kDa mMBP       HGRTQDENPV VHFFKNIVTP RTPPPSQGK             GAEGQKPGFG
18.5  kDa mMBP  74> HGRTQDENPV VHFFKNIVTP RTPPPSQGKG RGLSLSRFSW GAEGQKPGFG
18.5  kDa rmC1  74> HGRTQDENPV VHFFKNIVTP RTPPPSQGKG RGLSLSRFSW GAEGQKPGFG
18.5  kDa rmC8  74> HGRTQDENPV VHFFKNIVTP RTPPPSQGKG RGLSLSRFSW GAEGQQPGFG
17.24 kDa mMBP       HGRTQDENPV VHFFKNIVTP RTPPPSQGK             GAEGQKPGFG
17.22 kDa mMBP       HGRTQDENPV VHFFKNIVTP RTPPPSQGKG RGLSLSRFSW
14.0  kDa mMBP       HGRTQDENPV VHFFKNIVTP RTPPPSQGKG RGLSLSRFSW
                        .........exon-III][exon-IV..IV][exon-V...V] [exon-VI..

                        ........................exon-VI][exon-VII..VII]
21.5  kDa mMBP       YGGRASDYKS AHKGFKGAYD AQGTLSKIFK LGGRDSRSGS PMARR (194 aa)
20.2  kDa mMBP       YGGRASDYKS AHKGFKGAYD AQGTLSKIFK LGGRDSRSGS PMARR (183 aa)
18.5  kDa mMBP 124> YGGRASDYKS AHKGFKGAYD AQGTLSKIFK LGGRDSRSGS PMARR (168 aa)
18.5  kDa rmC1 124> YGGRASDYRS AHKGFKGAYD AQGTLSKIFK LGGRDSRSGS PMARR LEH6
18.5  kDa rmC8 124> YGGQASDYRS AHKGFKGAYD AQGTLSKIFK LGGQDSRSGS PMARQ LEH6
17.24 kDa mMBP       YGGRASDYKS AHKGFKGAYD AQGTLSKIFK LGGRDSRSGS PMARR (157 aa)
17.22 kDa mMBP                                          GGRDSRSGS PMARR (153 aa)
14.0  kDa mMBP                                          GGRDSRSGS PMARR (127 aa)
                        ........................exon-VI][exon-VII..VII]
```

FIGURE 1: Amino acid sequences of the "classic" murine MBP splice isoforms, ranging in size from 14 to 21.5 kDa. The classic exons are denoted by Roman numerals. The numbers at the beginning of each line for the 18.5 kDa isoform sequence are used for numbering. Since the N-terminal methionyl residue is cleaved in these proteins, it is numbered zero. The putative SH3 domain binding site is shown in boldface type. The arginyl/lysyl residues in the rmC1 isoform substituted by glutamine to yield the quasi-deiminated rmC8 variant are shown in boldface type and underlined. The peptide used for circular dichroism is outlined by a box.

MBPs from tss1 may be involved in regulation of neurogenesis and myelination and are implicated in remyelination in the human neurodegenerative disease multiple sclerosis (*1*, *4*). Posttranslational modifications of MBP generate considerable further microheterogeneity. Three major modifications of classic MBP of interest are deimination, phosphorylation, and methylation, whose levels change during both myelin development and the pathogenesis of multiple sclerosis (*5*−*8*). The various posttranslational modifications of MBP have been shown to affect its targeting to microdomains in myelin in vivo, as well as to modify its (local) conformation and modulate its interactions with lipid membranes and proteins such as calmodulin, actin, and tubulin (*2*, *3*, *7*, *9*−*19*).

Why this extensive posttranslational modification? It has been postulated that "multisite modification on a protein constitutes a complex regulatory program that resembles a 'dynamic molecular barcode' and transduces information to and from signaling pathways" (*20*), an idea recently reviewed further elsewhere (*21*). Moreover, all known forms of MBP fall into the "intrinsically disordered" or "conformationally adaptable" class, which comprises many signaling molecules (*22*−*25*). Such proteins have a large intermolecular interface and a relatively high net charge, being thus designed to interact with a plethora of ligands, often acting as hubs in interaction networks (*26*−*28*). Phosphorylation is also a leitmotif in the functions of such proteins (*29*, *30*). The extensive diversity of the MBP family, both genetic and posttranslational, and its conformational adaptability suggest that MBP is more than just a membrane adhesive in the central nervous system; it may modulate the local physicochemical properties of the myelin membrane and the assembly of the underlying cytoskeleton (*2*, *3*, *11*, *13*, *15*−*17*, *31*−*33*). In this sense, MBP has many physicochemical and phenomenological similarities to other intrinsically unstructured, cytoskeletal assembly proteins such as MARCKS,

tau, and microtubule-associated protein 2c (MAP-2c) (*34*−*36*).

However, the known interactions of MBP with the myelin membrane and with the proteins calmodulin, actin, and tubulin may represent an indirect (passive) signaling role in terms of modifying a local milieu. A direct interaction of MBP with signaling molecules would indicate an active role in myelin signaling. In Figure 1, we see that there is a potential SH3 domain target (TPRTP) in the classic MBP protein sequence, as has been previously noted (*37*, *38*). The SH3 domains are small conserved protein modules about 60 residues in size (*39*−*46*) that interact with relatively low affinity with a diverse range of proline-rich ligands (*41*, *46*−*55*), which are minimally an XP-x-XP consensus sequence that forms a left-handed polyproline type II (PPII) helix (*56*−*58*). These SH3 domains are found in a large number of intracellular signaling proteins, including the nonreceptor tyrosine kinases (NRTKs). The NRTK Fyn is of particular interest because it participates directly in MBP gene expression and in compact myelin sheath formation in the central nervous system (*59*−*64*). In lipid rafts isolated from myelin, there is a colocalization of Fyn and Lyn with Golli and classic MBP isoforms (*14*, *65*). In late myelination and in mature myelin, there is a partitioning of MBP and phospho-Thr95-MBP (murine 18.5 kDa sequence numbering) into lipid rafts (*14*, *66*).

Here, we demonstrate by circular dichroic (CD) spectroscopy that the putative SH3 ligand of MBP forms a polyproline type II (PPII) helix in vitro. Using protein microarray and sedimentation assays, we show that full-length MBP binds various SH3 domains from several proteins and that membrane-associated MBP can also bind an SH3 domain. The tertiary structures of several SH3 domains, some complexed with ligands, are known from X-ray crystallography and NMR spectroscopy (*67*−*70*). We have thus been able to investigate the details of SH3 domain interactions with the putative target in MBP by molecular modeling and docking simulations in silico, as we have recently published for calmodulin and its various targets in MBP (*71*). The effects of posttranslational modifications (viz., phosphorylation, deimination, and methylation) were investigated both experimentally and by modeling.

MATERIALS AND METHODS

Circular Dichroism. Two 18-residue peptides encompassing the classic polyproline segment of MBP (outlined segment in Figure 1) were purchased from AnaSpec Inc. (San Jose, CA); the manufacturer denotes them as MBP(89−105) and MBP(89-98T-106). It should be noted that this manufacturer's designation is based on the human 18.5 kDa sequence numbering that includes the N-terminal methionyl residue as 1, even though it is actually cleaved posttranslationally (*72*, *73*), and that the numbering used in the literature always starts with the alanyl residue as 1 (*2*, *3*), which convention we shall follow here. The peptide sequence is FFKNIVTPRTPPPSQGKG and is identical in all mammals (*2*), corresponding to murine 18.5 kDa residues F86−G103 (cf. Figure 1). The second peptide was phosphorylated on residue T98 (human sequence, corresponding to residue T95 in the mouse protein.

CD spectroscopy was performed on a Jasco J-810 spectropolarimeter (Japan Scientific, Tokyo, Japan), equipped with a recirculating water bath. Samples were of 0.3 mL volume, in a 0.1 cm path-length quartz cuvette. The samples analyzed were of each peptide (0.3 mg/mL) in aqueous solution (10 mM Na phosphate and 10 mM KCl, pH 6.5), or the full-length recombinant murine 18.5 kDa protein (rmC1) (*73*), at 0.2 mg/mL in 100 mM KCl, pH 6.5). Measurements were taken at a 100 nm/min rate, at 0.1 nm intervals, over a range of 190−250 nm. Measurements were recorded at temperatures ranging from 5 to 65 °C in 5 °C increments. At each temperature, four successive scans were recorded, the sample blank was subtracted, and the scans were averaged. The data averaging and smoothing (by use of an inverse square algorithm) operations were accomplished with the SigmaPlot (SPSS, Chicago, IL) computer program.

Microarray and Sedimentation Assays: (A) Materials. The least modified, most highly positively charged 18.5 kDa isoform of MBP, bC1, was purified from bovine brain MBP as described (*74*). Expression constructs containing cDNA for murine 18.5 kDa MBP (rmC1) and quasi-deiminated MBP (rmC8) in pET22b(+) vectors (Novagen), were transformed into and expressed in *Escherichia coli* BL21-CodonPlus(DE3)-RP (Stratagene) (*73*, *75*). Recombinant murine 18.5 kDa MBP rmC1 is unmodified, save for an LEH_6 tag (*73*). The variant rmC8 was generated from rmC1 by sequential site-directed mutations (first R25Q, then R33Q, K119Q, R127Q, R157Q, and finally R168Q, murine sequence numbering) via the QuikChange protocol (Stratagene, La Jolla, CA) as described previously (*75*). Both recombinant variants were purified via nickel-chelation chromatography with Ni^{2+}−NTA agarose beads (Qiagen, Mississauga, ON). The proteins bC1 and rmC1 were phosphorylated with recombinant p42 MAPK (New England Biolabs) at Thr94 and Thr97 (bovine sequence) and at Thr92 and Thr95 (murine sequence) as described (*17*), yielding Ph-bC1 and Ph-rmC1, respectively. Electrophoresis on alkaline tube gels (*17*) indicated that rmC1 yielded mostly singly phosphorylated protein, whereas bC1 yielded mostly doubly phosphorylated protein. The SH3 domain of Fyn, residues 85−142, containing a FLAG epitope and a His_6 tag at the C-terminus and a short N-terminal tail, was a kind gift from Dr. Alan Davidson, University of Toronto, and was prepared and purified as described (*76*).

Egg L-*R*-phosphatidylcholine (PC) and L-*R*-phosphatidylglycerol (PG; prepared from egg PC) were purchased from Avanti Polar Lipids, Inc. (Alabaster, AL). [^{3}H]Cholesterol was from Amersham (Baie d'Urfe, QC, Canada).

(B) Preparation of Large Multilamellar Vesicles. Aliquots of chloroform/methanol (2:1) solutions of the lipids were combined to give a PC/PG mole ratio of 8.5:1.5. [^{3}H]-Cholesterol was added to give a specific activity of 100 000 cpm/10 μmol of lipid. The solvent was evaporated under a stream of nitrogen with the tube maintained at room temperature in a water bath, and the lipid film was evacuated in a lyophilizer for 2 h. The dry lipid film was dissolved in 1−2 mL of benzene, frozen, and lyophilized overnight. The lipid (2 mg) was hydrated in 1 mL of 5 mM Tris-HCl buffer containing 0.2 mM $CaCl_2$, 50 mM KCl, 2 mM $MgCl_2$, 1 mM ATP, and 0.5 mM dithiothreitol at pH 7.5 (buffer A). Multilamellar vesicles (MLVs) were prepared by freeze−thawing five times in a dry ice/acetone bath followed by a 40 °C water bath, and dispersing the lipid by vigorous vortex mixing.

(C) Fyn SH3 Domain Binding to Liposome-Associated MBP Charge Isomers. The MBP isomers bC1 (natural bovine 18.5 kDa C1 component), Ph-bC1, and rmC8 were dissolved in distilled water at a concentration of 2 mg/mL, and the Fyn SH3 domain was supplied in 50 mM phosphate buffer containing 100 mM NaCl at pH 7.0 at a concentration of 1.74 mg/mL. An aliquot of each MBP sample (50 μg) was added to an aliquot of MLVs (500 μg) and mixed gently, and the mixture was incubated for 10 min at room temperature. Aliquots of the Fyn SH3 domain were added (giving initial molar ratios of Fyn SH3 domain to bC1 of 2.2−6.5 and to Ph-bC1 and rmC8 of 2.2), and the sample was made up to a total volume of 0.5 mL in buffer A and was incubated for a further 1 h at room temperature. A control sample without MBP was prepared similarly. The samples were centrifuged at 11800*g* for 15 min at 4 °C in an Eppendorf bench centrifuge. The supernatant was removed; the pellet was washed gently by addition of 0.4 mL of buffer, without mixing, and was then resuspended in a fresh aliquot of 0.4 mL of buffer. Aliquots of the supernatant and resuspended pellet were taken for counting of [^{3}H]cholesterol, for protein assay by the Peterson method (*77*), and for gel electrophoresis on 10% Bis-Tris NuPage gels (Invitrogen, Mississauga, ON, Canada) along with standards of bC1 and Fyn SH3. Coomassie blue-stained gels were analyzed with a UVP image analyzer (UVP, Upland, CA), and band areas were compared to those of the standards in order to quantitate the amount of each protein in the sample. Band densities were within the linear range.

(D) Binding of rmC1, Ph-rmC1, and rmC8 to SH3 Domains on a Microarray. The binding of rmC1, phosphorylated rmC1 (Ph-rmC1), and rmC8 to a TransSignal SH3 domain array I (Panomics, Redwood City, CA) was determined by incubation of the membrane filters with 15 μg/mL rmC1, Ph-rmC1, or rmC8, in the blocking buffer provided in the kit according to the manufacturer's instructions. After washing, bound protein was detected by incubation with HRP-conjugated anti-His antibody, provided in the kit.

Molecular Modeling: (A) Software. For docking simulations, the peptides were constructed as described below by use of the program SYBYL version 7.0 (SYBYL, Tripos Associated Inc., St. Louis, MO; cf. ref *78*), and energy-minimized by use of the Tripos force field (*79*). Such computations were performed on an SGI Octane R12000 running IRIX 6.5 (Silicon Graphics Inc., Mountain View, CA). The lengths of the peptides were kept as small as possible, while the requisite binding characteristics were retained, in order to minimize calculation time.

(B) Choice of SH3 Domain Structure. The choice of the SH3 domain structure to use for the docking simulations was made on the basis of several considerations. Because the Fyn NRTK plays a major role in central nervous system myelination and contains an SH3 domain, we sought a convenient structure for the SH3 domain among the crystal structures available for Fyn (all from human Fyn) in the Protein Data Bank (*80*). After a careful analysis and comparison, we chose the crystal structure 1shf, chain A, because it was complete and had the best resolution, 1.9 Å (*67*). The torsion angle of the side chain of Tyr91 (a residue that is usually involved in the interaction with the ligand) of 1shf was modified according to the conformation that it has in the other crystal structures of human Fyn.

(C) Building of MBP Peptide. The potential SH3 target in the classic MBP isoforms [murine 18.5 kDa MBP(T92−P96) = TPRTP] (Figure 1) presents the known core motif XP-x-XP and is of interest because of the various serine and threonine phosphorylation sites and the arginine methylation site in its vicinity, as will be discussed below. Here, we modeled the structure of an opportune segment ($T^{1'}$ $P^{2'}$ $R^{3'}$ $T^{4'}$ $P^{5'}$ $P^{6'}$ $P^{7'}$ $S^{8'}$ $Q^{9'}$ $G^{10'}$ $K^{11'}$ $G^{12'}$ $R^{13'}$; residues T92−R104 in the murine 18.5 kDa MBP sequence), following the typical Fyn SH3 ligand characteristics. With the SYBYL software, we built the backbone of the residues from $T^{1'}$ to $P^{7'}$ in a PPII conformation ($\varphi = -78°$ and $\varphi = +149°$). This choice was driven by the reported structural characteristics of the SH3 domain ligands (*40*, *81*), deduced from the experimentally resolved structures, and is in agreement with our CD results. The torsion angles of the side chains of the $T^{1'}$−$P^{7'}$ segment were left free to rotate in the docking simulations. The residues from $S^{8'}$ to $R^{13'}$ were temporarily built in an extended conformation; however, backbone and side-chain torsion angles were completely free to rotate in the docking simulations. The overall conformation of the constructed peptide was at first relaxed by a moderate energy minimization.

(D) Posttranslational Modifications of the Ligands. Posttranslational modifications (phosphorylation and methylation) were performed in silico, building on our previous experience with MBP−calmodulin modeling (*71*). First, the unmodified ligand was docked, and the best structure obtained from this simulation was then modified. The modified ligands were then docked to the SH3 domain and left free to change their conformation and position with the same degrees of freedom of the unmodified peptide. The following six modifications were individually applied: the residue $S^{8'}$ was modified to PhS (phosphorylated serine), the residues $T^{1'}$ and $T^{4'}$ were modified to PhT (phosphorylated threonine), and finally the residue $R^{13'}$ was monomethylated (MM), asymmetrically dimethylated (ADM), and symmetrically dimethylated (SDM).

The PhS residue is included in the nonstandard amino acid molecular library of the SYBYL program; therefore, the attribution to each atom of its partial charges was made according to Kollman (*82*), as is usual for a peptidic ligand. The $T^{1'}$, $T^{4'}$, and $R^{13'}$ modifications were constructed, always with the SYBYL software, and the calculation of partial charge for the atoms of modified peptides was made according to Gasteiger (*83*), as is usual for a generic ligand. To check if the different charge attributions could lead to different results, we first performed two docking simulations on the unmodified MBP peptide, with both the Kollman and Gasteiger partial charges sets.

Molecular Docking Simulations. Simulations of the interaction of MBP unmodifed and modified peptides with the SH3 domain were performed with the Autodock3 software package (*84*) with the aid of the AutoDockTools (ADT) interface, running on a PC cluster (AMD Opteron 64 bit). For the docking calculations, the Lamarckian genetic algorithm (*84*) was used.

In all the simulations, the backbone torsion angles of the PPII region (residues $T^{1'}$−$P^{7'}$) were kept constant (although the side chains were flexible), whereas the flanking region was completely flexible (both the backbone and the side-

Table 1: Summary of Docking Simulations

docking simulation	modification	partial charge set	docked energy of best structure[a] (kcal/mol)	median value of energy histogram[b] (kcal/mol)
ds1a	none	Kollman	−18.8	−14.8
ds1b	none	Gasteiger	−18.6	−14.9
ds2	$S^{8'} \rightarrow PhS^{8'}$	Kollman	−16.2	−11.0
ds3a	$T^{4'} \rightarrow PhT^{4'}$	Gasteiger	−17.2	−13.2
ds3b	$T^{1'} \rightarrow PhT^{1'} + T^{4'} \rightarrow PhT^{4'}$	Gasteiger	−15.9	−12.1
ds4	$R^{13'} \rightarrow R^{13'}$-MM	Gasteiger	−18.5	−14.6
ds5	$R^{13'} \rightarrow R^{13'}$-ADM	Gasteiger	−18.3	−14.9
ds6	$R^{13'} \rightarrow R^{13'}$-SDM	Gasteiger	−18.4	−14.5

[a] Best complexes with the unmodified and modified MBP peptides. [b] See Figure 5.

chain torsion angles could vary). In this way, during the conformational search, not only were all all of the torsion angles free to rotate, but also the whole peptide could change its orientation and explore the space around the binding site, defined by the grid dimensions.

Preliminary Test Simulation and Docking Parameters Setting. A preliminary test simulation was performed on the structure 1azg (*70*), which is a minimized average NMR structure of the Fyn SH3 domain complexed with a Pro-rich peptide (PPRPLPVAPGSSKT, residues P91−T104) from subunit P85 of PI3 kinase. The SH3 domain structure and the PI3 peptide initial coordinates were extracted from the original 1azg PDB file and some docking tests were performed between them, in order to check if the right complex was correctly identified by the docking algorithm and to set the best simulation parameters for obtaining a correct result. This step permitted the use of such parameters for a similar ligand (the MBP peptide) with the same high number of degrees of freedom, docked into the analogous binding site of the 1shf crystal structure of the SH3 domain. Similar to the MBP peptides, the PI3 ligand torsion angles were left flexible with the exception of the backbone torsion angles of the first nine residues, which were in a PPII conformation. The choice of the 1azg ligand peptide for the docking test was made because the ligand peptide is part of a natural protein, PI3 kinase, and because it is 14 residues long, just one amino acid longer than our MBP peptide; therefore, the degrees of freedom are comparable.

On the basis of the good results obtained with this test peptide, the following docking parameters were chosen for all the other simulations with the MBP peptide: the number of individuals in the population was 300, the maximum number of energy evaluations was 25 000 000, and the number of runs was 200. For the other docking parameters, the default settings were used. The docking simulations that were run subsequently between the unmodified and modified MBP peptides and the SH3 domain are denoted **ds1**−**ds6** and are summarized in Table 1.

For **ds1a** and **ds1b**, a grid with a spacing of 0.5 Å and dimensions of 80, 78, and 74 points (in the *x*, *y*, and *z* directions, respectively) was initially used. Then the best conformation obtained was optimized with a grid spacing of 0.375 and with (*x*, *y*, *z*) dimensions of 100, 86, and 94 points. The latter grid parameters were used for all the subsequent simulations with the modified peptides.

For each simulation, the resulting complexes were clustered with a threshold of 3 Å rmsd (root mean squared deviation) for ligand structure similarity. Then, we compared the structure with the absolute lowest docked energy and the structure with the lowest docked energy in the more populated cluster to choose the best conformation for the analyis.

Structures were examined with the ADT interface in Autodock (*84*), SwissPdbViewer (*85*), and RasMol (*86*) software packages. The "contact residues" of the SH3 domain with the ligand were assigned by means of the FirstGlance in Jmol program (at http://molvis.sdsc.edu/fgij/index.htm, copyright 2005, 2006 by Eric Martz). The CH···π interactions were identified on the basis of geometric criteria (*87*). All figures were drawn with the ViewerLite 5.0 (Accelrys Software Inc., San Diego, CA) software package.

RESULTS AND DISCUSSION

MBP Possesses a Putative SH3 Domain Ligand. The classic MBP isoforms all possess a highly conserved, putative SH3 ligand: T92-P93-R94-T95-P96 (murine 18.5 kDa sequence numbering, unless otherwise noted) (Figure 1). This motif is encoded by classic exon IV and is contained in all six known classic MBP isoforms, as well as in the Golli-MBP isoform J37 (*1*, *88*). The murine Golli-MBP isoforms J37 (*88*) and BG21 (*89*) contain an additional potential SH3 target [Golli(H80−P84) = HPADP], but we focused here on the classic site because the various posttranslational modifications within it and nearby have been better documented. The segment immediately preceding this motif, P82VVHFFKNIVTP93, is an immunodominant epitope of MBP and forms an amphipathic, surface-embedded, α-helix (*90*, *91*). The residues P93 (one of the two prolyl residues flanking the α-helix) and S99 are exposed to the cytoplasm (*90*, *92*), suggesting that the putative SH3 ligand should be oriented outside the membrane where it would be accessible to other modifying or recognition proteins.

Within the immunodominant epitope (P82−P93), the only residue modified is T92, which is a secondary mitogen-activated protein kinase (MAPK) site (*93*). The residue T95 within the putative SH3 ligand is a primary MAPK and glycogen synthase kinase 3β (GSK-3β) site (*94*, *95*), and MBP modified here is associated with lipid rafts (putative signaling platforms) in mature myelin (*14*, *19*, *66*). It has been suggested that interaction of proteins such as tau with an SH3-domain-containing protein might direct them to lipid rafts (*35*). Residue R94 is a potential secondary deimination site (albeit not in rmC8, which contains primary deimination sites), whereas S99 is phosphorylated by protein kinase C (*2*, *5*). Slightly further downstream, R104 is either unmodifed, monomethylated (ω-N^G-monomethyl-Arg), or symmetrically dimethylated (ω-N^G,N'^G-dimethyl-Arg) (*2*, *5*). Most proteins have an asymmetric dimethylarginine, so MBP is unusual in that it has a *symmetric* dimethylarginine. Regardless, in some cases, the methyl group causes steric hindrance in interactions with SH3-domain-containing and other proteins (*96*−*99*), and in MBP it is thought to interfere with deimination by peptidylarginine deiminase (*7*, *100*). Thus, methylation and phosphorylation of MBP, especially in the vicinity of the putative SH3 ligand, might affect its local conformation (*9*, *10*) and binding to SH3 domains, as is the case for other proteins such as tau and other microtubule-associated proteins (*99*, *101*, *102*).

Polyproline Type II Helix in MBP. Polyproline type II helices are characterized by the average backbone (φ, ψ) dihedral angles of (−75°, +145°), resulting in a left-handed, all-trans, extended helix of approximately 3.12 Å in length per residue (*58*). One complete turn of the helix will span approximately 9 Å, giving the helix 3-fold rotational symmetry. Due to this extended arrangement, the residues that participate in the helix are precluded from forming stabilizing interresidue interactions; that is, there are no N−H···O hydrogen bonds. Thus, PPII helices are often confined to short stretches of amino acids and are prevalent in disordered proteins (*103*, *104*); indeed, they are considered to exist as one of many conformational states (*105*). Until recently, the CD spectra of PPII-containing proteins have been interpreted as "random coil", whereas a closer investigation reveals the underlying subtleties (*106*).

Since the CD spectra of polypeptides in the PPII conformation are similar to those of unfolded polypeptides (*107*, *108*), they are best discerned by comparing them over a range of temperatures (*109*, *110*), as is demonstrated here for an MBP polypeptide encompassing the proline-rich segment (Figure 2). A temperature difference presentation is required since part of the peptide may form a segment of an amphipathic α-helix (*91*) under these conditions. This would mask the characteristic positive transition at 222 nm, making it difficult to discern the PPII character. Thus a temperature-difference spectrum allows for the "amplification" of the signal from the PPII helix. Here, phosphorylation of the residue corresponding to murine Thr95 (a MAP kinase target) results in conformational stabilization (Figure 2E,F) compared with the unmodified peptide (Figure 2C,D). Specifically, the 45 °C trace for the phosphorylated peptide (Figure 2E, ···) is still comparable to the traces at lower temperatures, whereas the 45 °C trace for the unmodified peptide is more comparable to the higher temperature traces, which show a greater degree of disordered conformation (Figure 2C, ···). The difference between the two peptides may be due to a stabilizing effect of phosphorylation, by interaction of the phosphate with backbone amide groups (*111*). These CD results thus suggest that this proline-rich segment of MBP can, indeed, form a PPII helix under physiological conditions.

In the full-length protein (Figure 2A,B), the lack of observable temperature-induced disorder in the spectra at elevated temperatures may be due to stabilization by the higher salt concentration or by local hydrophobic interactions. At 65 °C, full-length MBP still retains the classic intrinsically disordered profile (with minima at approximately 200 nm), whereas the peptides have almost a flat profile (random coil). A strictly qualitative interpretation suggests that full-length MBP is able to maintain a higher degree of order (on average) than the peptides at temperatures greater than physiological temperature, due to other interactions or stabilization forces that are lacking in the peptides.

It has been shown by site-directed spin-labeling and electron paramagnetic resonance spectroscopy that both flanking segments are membrane-associated (*92*); the preceding immunodominant epitope is a surface-associated α-helix, and some downstream C-terminal residues insert into the membrane; however, the proline-rich segment is exposed in the cytoplasm to ionic conditions like those under which we performed the CD experiments, and it is likely that the PPII conformation also exists in vivo (*103*−*105*). The exon-II-containing isoforms of classic MBP are nuclear-localized (e.g., the 21.5 kDa isoform, Figure 1), and the proline-rich segment may also function as a flexible hinge (*112*) in these cases. Pioneering NMR work on similar MBP-derived polypeptides indicated that all prolyl residues were in trans form (*113*, *114*). This region could thus not form a hairpin bend unless one of the prolyl residues isomerized to the cis form, which would in turn cause the polypeptide chain to be redirected substantially, and/or render this segment a more (or less) suitable target for specific kinases (which can be either cis- or trans-specific) or phosphatases (generally trans-specific) (*115*).

The potential trans → cis isomerization of prolyl residues in MBP in vivo would involve an interplay of several factors. First, the spontaneous rate of isomerization is very slow and almost negligible and has been seen to increase to about 5% in the membrane-associated protein (*114*). Phosphorylation of the threonyl residues within the TP-R-TP motif would stabilize the backbone conformation and slow the rate of spontaneous isomerization (*9*, *10*, *111*). Phosphorylation of these threonyl residues may result in a localized detachment of the C-terminus of this amphipathic α-helix from the phospholipid membrane, a phenomenon similar to what has been observed for the deiminated protein (*18*, *116*). Alternatively, there are prolyl isomerases (e.g., Pin1) that efficiently isomerize phosphorylated Ser/Thr−Pro bonds in certain proteins, as a novel signaling mechanism (*115*, *117*−*119*). These isomerases have been identified in neurons, and their presence in myelin remains to be determined.

MBP Binds SH3-Domain-Containing Proteins. Preliminary experimental investigations with dot-blot and pull-down (affinity precipitation) assays have previously shown that 18.5 kDa MBP interacts in vitro with several SH3-domain-containing proteins, such as Fyn (*38*). Here, we report a more extensive and semiquantitative screen using microarrays and recombinant murine MBP (Figure 3), sedimentation assays with the natural bovine 18.5 kDa MBP associated with lipid vesicles (Figure 4), and the effects of phosphorylation by MAPK and arginine deimination of MBP on the interaction with SH3 domains.

Recombinant murine forms rmC1, rmC8, and Ph-rmC1 bound to the GST SH3 domains of a number of proteins on a membrane array (*120*) significantly more strongly than to GST (Figure 3). The HRP reagent reacted only with the positive controls along the bottom and side edges of the array (not shown in Figure 3). Of those SH3 domains for which binding to rmC1 (net charge +19 at neutral pH) was strongest, binding decreased in the order Yes1 > PSD95 > PexD = cortactin = Abl = Itk = c-Src = Fyn. Binding to rmC8 (net charge +13 at neutral pH) decreased in the order Yes1 > Fyn > cortactin = c-Src > PexD = Abl. Notably, rmC8 did not bind to PSD95 or Itk, in contrast to rmC1. Since R94 on the 18.5 kDa murine MBP rmC8 form is not modified (quasi-deiminated) (*75*), this result indicates a global effect of deimination of other regions of MBP on interaction of its P93-RT-P96 site with SH3 domains, as has been observed previously for MBP and calmodulin (*12*, *121*). Phosphorylation of Thr92 and/or Thr95 of rmC1 by MAPK did not result in any noticeable change in the binding specificity of MBP for the SH3 domains on the array.

The recombinant form of the SH3 domain of chicken Fyn in solution also bound to the natural form of bovine 18.5

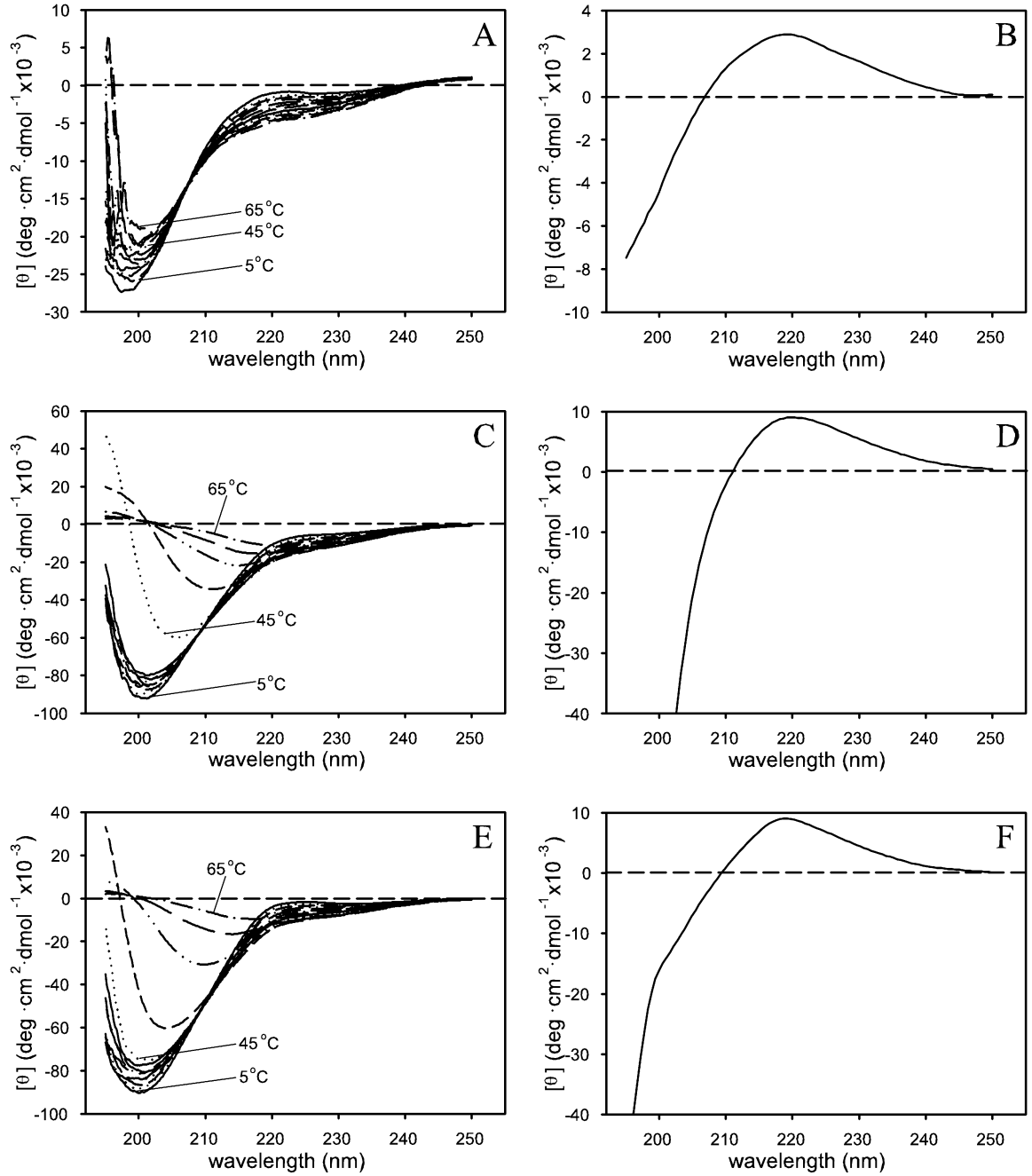

FIGURE 2: Circular dichroic spectra for (A, B) full-length recombinant murine 18.5 kDa MBP, (C, D) Anaspec MBP(90−106) peptide, and (E, F) Anaspec MBP(90-99P-106) peptide. The peptide sequence is identical to murine 18.5 kDa residues F86−G103 (Figure 1). Spectra in panels A, C, and E were obtained by increasing the temperature from 5 to 65 °C in 5 °C increments. Panels B, D, and F each show a difference spectrum obtained by subtracting the corresponding 45 °C spectrum from the 5 °C spectrum. The difference spectra for the full-length protein (panel B), and especially for both peptides (panels D and F), have a positive maximum at about 220 nm, indicative of a polyproline type-II helix. The PPII helical character is lost with increasing temperature due to the absence of interresidue hydrogen bonding. An isodichroic (isoelliptic) point at approximately 210 nm (panels A, C, and E) suggests that there is a two-state equilibrium between the left-handed PPII helix and the disordered chain, consistent with the transient nature of PPII helices.

kDa MBP/C1 (bC1) on the outer surface of negatively charged PC/PG (8.5/1.5 mol/mol) lipid vesicles. The protein bC1 binds strongly by electrostatic interactions to these lipid vesicles. Figure 4A shows that both bC1 and the Fyn SH3 domain were found in the lipid−protein pellet (lanes 1−3). If bC1 was not present, the Fyn SH3 domain did not bind to the lipid pellet (lane 4). When the initial molar ratio of the Fyn SH3 domain to bC1 was 2.2, the molar ratio of the Fyn SH3 domain to bC1 bound to the lipid vesicles was unity (lane 1). No further binding of the Fyn SH3 domain occurred at higher molar ratios. Although Fyn SH3 contained a His_6 tag, we were not able to measure binding of bC1 to it on a Ni^{2+}−NTA agarose column because bC1 binds by itself to the column. At an initial molar ratio of the Fyn SH3 domain to modified MBP isomers of 2.2, the molar ratio of Fyn SH3 bound to Ph-bC1 was 0.6 and that to rmC8 was 1 (Figure 4B). Thus phosphorylation and deimination of bC1 had little apparent effect on binding of the Fyn SH3 domain.

Features of the SH3 Domain. The SH3 domain fold is highly conserved and is composed of five β-strands organized into two β-sheets packed at right angles to form a sandwich. The second β-strand, βB, is shared between the two sheets,

A **Configuration of SH3 Domain Array I**

Amp	LCK	SPCN	Cortactin	MLPK3	Yes1	Abl2	SJHUA	Itk	CRKD2
Dlg2	EMP55	FGR	SLK	Nebulin	cSrc	FYBD1	Hck	VAV2D2	NOF2D1
VAVD1	NCK1D3	Y124	PEXD	BTK	RasGAP	PSD95	Tim	HS1	Stam
BLK	Abl	PLCγ	Riz	PI3β	ITSND1	ITSND2	TXK	GST	

B

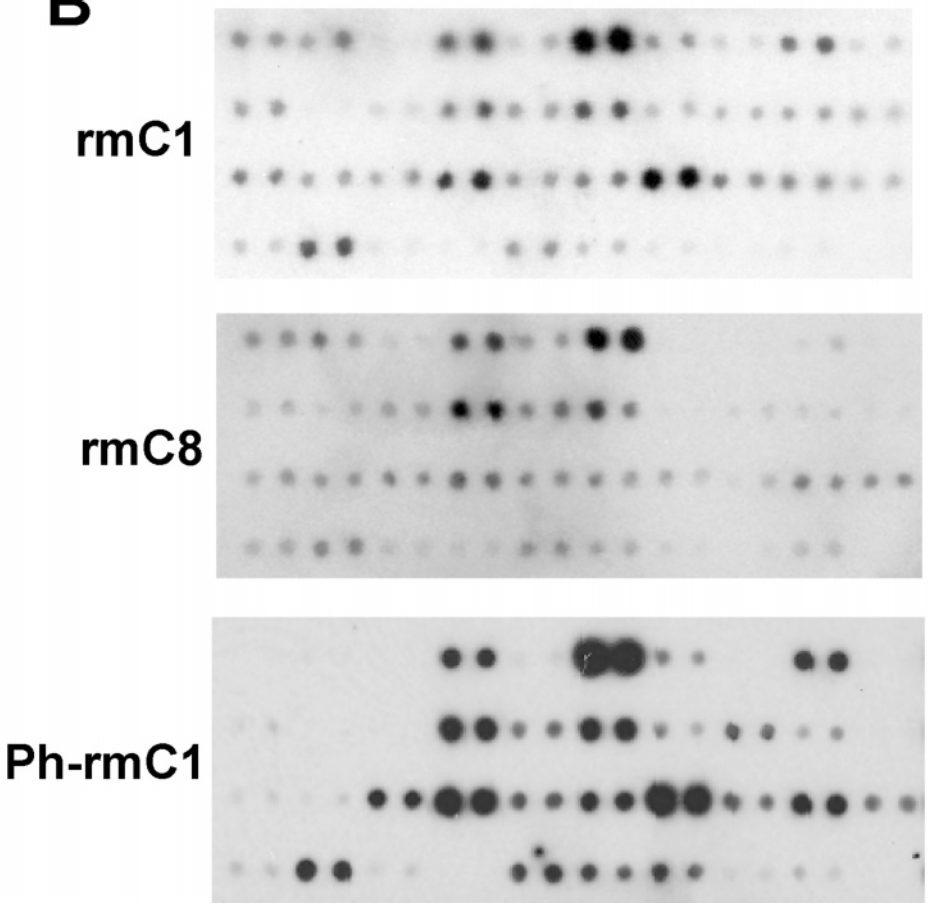

FIGURE 3: Recombinant murine 18.5 kDa isoforms rmC1 and rmC8 bound to a subset of SH3 domains. A Panomics Array I of GST−SH3 domain fusion proteins was probed with His_6-tagged rmC1 and rmC8 and HRP-conjugated anti-His antibody. (A) Configuration of protein array. Each GST−SH3 domain was spotted in duplicate. (B) Binding of rmC1, rmC8, and Ph-rmC1 to the microarray as detected on film via chemiluminescence. Binding to GST alone was much weaker. The same solution of rmC1 as used for phosphorylation was used for panel B. Representative arrays are shown. The SH3 domains on the array were amphiphysin, Discs large homologue 2 or MAGUK P55 subfamily member 2 (Dig2), VAV proto-oncogene SH3 domain 1 (VAV-D1), β-lymphocyte-specific protein tyrosine kinase (BLK), human T-lymphocyte-specific protein tyrosine kinase p56 LCK (LCK), 55 kDa erythrocyte membrane protein (EMP55), cytoplasmic protein NCK1 SH3 domain 3 (NCK1-D3), Abelson tyrosine kinase (Abl), nonerythrocytic spectrin α-chain (SPCN), cellular Gardner−Rasheed feline sarcoma virus protein (FGR), PAK-interacting exchange factor-β (Y124), phospholipase Cγ-1 (PLCr), Src substrate cortactin, proto-oncogene tyrosine protein kinase Fyn (SLK), peroxisomal membrane protein PEX13 (PEXD), retinoblastoma protein-interacting zinc finger (Riz), mixed-lineage kinase 3 (MLPK3), nebulin, tyrosine-protein kinase BTK (BTK), phosphatidylinositol 3-kinase regulatory β-subunit (PI3β), Yamaguchi sarcoma virus oncogene homologue 1 (Yes1), cellular Rous sarcoma viral oncogene homologue (c-Src), Ras GTPase-activating protein 1 (RasGAP), intersectin 1 SH3 domain 1 (ITSN-D1), Abelson-related protein (Abl2), Fyn-binding protein SH3 domain 1 (FYB-D1), presynaptic density protein 95 (PSD95), intersectin 1 SH3 domain 2 (ITSN-D2), erythrocytic spectrin α-chain (SJHUA), hematopoietic cell kinase (Hck), ρguanine nucleotide exchange factor 5 (Tim), tyrosine protein kinase TXK (TXK), interleukin-2-inducible T-cell kinase (Itk), VAV-2 protein SH3 domain 2 (VAV2-D2), hematopoietic-specific protein (HS1), glutathione S-transferase (GST), avian sarcoma virus CT10 oncogene homologue SH3 domain 2 (CRK-D2), neutrophil cytosol factor 2 SH3 domain 1 (NOF2-D1), and signal-transducing adaptor molecule (Stam).

possessing a kink that changes the direction of the polypeptide. One side of the sandwich is rather hydrophobic and constitutes the ligand-binding surface. It is delimited on one side by an RT loop between the βA and βB strands (residues Glu94−Ser102, following human Fyn SH3 domain numbering), and on the other side by a small loop between the βB

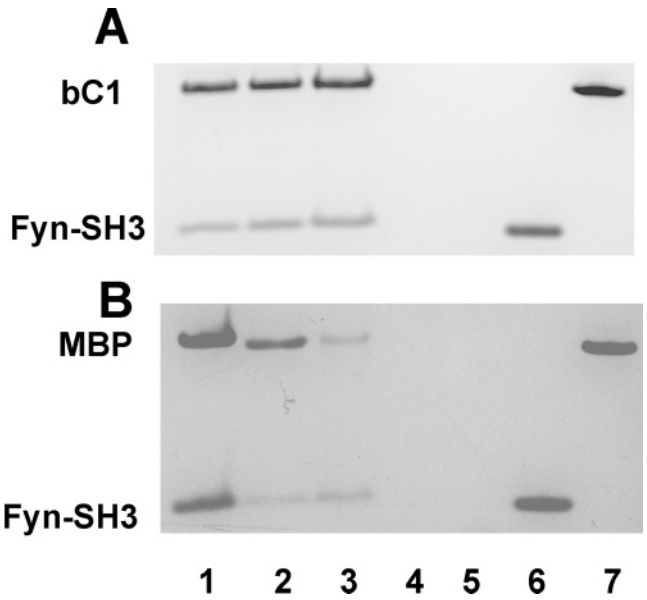

FIGURE 4: (A) Fyn SH3 domain bound to PC/PG (8.5/1.5 mol/mol) lipid vesicles in the presence of the natural bovine 18.5 kDa MBP isomer bC1 (lanes 1−3) but not in its absence (lane 4). The lipid−protein pellet sedimented at 11800*g* and was resuspended and run on the gel. Lane 5 is blank. Protein standards are 1.75 μg of Fyn SH3 domain (lane 6) and 2 μg of bC1 (lane 7). The mole ratio of Fyn SH3 to bC1 added to the vesicles was 2.2 (lane 1), 4.3 (lane 2), and 6.5 (lane 3). The mole ratio of Fyn SH3 to bC1 recovered in the pellet was determined by densitometry and comparison to the standards. (B) Less Fyn SH3 domain bound to PC/PG (8.7/1.3 mol/mol) lipid vesicles in the presence of Ph-bC1 (lane 2) than bC1 (lane 1). Fyn SH3 domain bound similarly to the lipid vesicles in the presence of rmC8 (lane 3) as bC1. The initial mole ratio of Fyn SH3 domain to MBP added to the vesicles was 2.2 in all cases. Fyn SH3 domain did not bind to the lipid vesicles in the absence of MBP (lane 4). Equal amounts of lipid pellet were run on the gel for lanes 1−4. Less Ph-bC1 and rmC8 bound to the lipid vesicles under these conditions than bC1. Lane 5 is blank. Protein standards are 0.9 μg of Fyn SH3 domain (lane 6) and 1.0 μg of bC1 (lane 7). The mole ratio of Fyn SH3 to MBP charge isomer recovered in the pellet was determined by densitometry and comparison to the standards.

and βC strands (called the n-Src insertion point loop, residues Ser114−Trp119) and by a five-residue-long 3_{10} helix (Ser135−Tyr137), which separates the βD and βE strands.

Numerous aromatic amino acids are present in the binding surface, viz., Tyr132, Trp119, Tyr137, Tyr91, and Tyr93. Cesareni et al. (*81*) identified hydrophobic pockets formed by the residues AL(YF)D(YF) (89−93), WW (119−120), and PXNY (134−137), although residues Ala89, Leu90, and Trp120 are quite far from the binding site. The first of these binding pockets in the SH3 domain is lined by negatively charged residues—Glu98, Asp99, and Asp100 in the RT loop; Glu116, Asp118, and Glu121 in the n-SRC loop; and Glu129 in the βD strand before the 3_{10} helix—and can host a positively charged side chain flanking the core motif in the ligand (see below).

The SH3 domain structure that we chose to use for the docking simulations was the 1shf Fyn structure, for reasons described above. Even though the 1shf structure was without any complexed ligand peptide, the comparison with other known SH3−peptide complexes confirmed that the presence of the ligand did not involve structural changes in the SH3 domain, as is generally the case (*46*). [It has recently been noted that ligand-binding actually stabilizes the SH3 domain structure (*122*).]

Features of SH3 Ligands. Canonical SH3 ligands usually contain two identical XP dipeptides, separated by a scaffolding residue (often a proline) (*40*−*42*, *46*, *50*, *81*). The two XP moieties in the core motif (XP-x-XP) occupy two of the hydrophobic pockets (see above), and a stacking interaction between one of the Pro residues and the Trp of the binding pocket is well-conserved. In fact, the proline residues of the ligand seem to be implicated in having a role in molecular association employing C−H$\cdots\pi$ interactions with aromatic residues at the binding site (*123*), of which the above-mentioned Pro-Trp stacking is well-conserved. Moreover, the interaction with the ligand is both hydrophobic (in particular between the conserved aromatic residues of the binding site of the SH3 domain and the aliphatic side chains of the ligand), and also mediated by hydrogen bonds (in particular those from the aromatic residues, as well as Asn136, of the binding site and the backbone oxygens of the ligand, which are characteristic) (*40*, *69*). The third SH3 domain binding pocket, lined by negatively charged residues, can host a positively charged side chain flanking the core motif, as indicated before. Usually, the positively charged residue interacts with the acidic cluster on the RT loop. The 7−9 amino acid core region of the ligand binds to SH3 receptors in a left-handed PPII helical conformation (*40*, *81*), in either of two opposite orientations depending on the position of a positively charged residue in the peptide sequence.

In Fyn and some other SH3 domains, the residue Arg/Ile96 (human Fyn numbering) in the RT loop seems to be the key for the selectivity and high affinity of the binding (*40*). Actually, in the analyzed PDB structures (see Table 2 below), this residue does not make any contacts directly with the core motif but only with the rest of the protein linked to it, if present [e.g., the Nef protein in PDB entries 1avz and 1efn (*124*, *125*)]. It has been reported that the flanking peptide region usually enhances the affinity and selectivity of ligand binding; therefore, the whole structure of the bound protein is important and not only that of the ligand peptide. There are, however, many exceptions to the general binding mode.

Docking Simulations of MBP Peptides to SH3 Domains. In order to set the correct parameters for a docking simulation with such a high number of degrees of freedom and to determine if the docking algorithm could find the favored binding complex, a preliminary test simulation was performed with the Fyn SH3 domain structure and the initial coordinates of the PI3 ligand, extracted from the 1azg PDB structure (see Materials and Methods). The family of 25 NMR structures deposited into the related file 1a0n (from which 1azg was obtained by averaging and minimization), demonstrate the flexibility in solution of the different structural regions of this type of SH3 domain ligand. This comparison reveals that the C-terminal region of the peptide is very flexible and can assume very different spatial orientations, whereas the N-terminal residues are in a PPII helix and remain in the same position in all the structures.

The docking test simulation recovered the correct complex conformation and not only allowed us to set the best docking parameters for subsequent runs, as indicated under Materials

Table 2: Residues of the SH3 Domain That Made Contacts with the Ligand[a]

	ds1a,b	ds2	ds3a	ds3b	ds4	ds5	ds6
canonical Fyn[b]	unmodified MBP	MBP PhS$^{8'}$	MBP PhT$^{4'}$	MBP PhT$^{1'}$ + PhT$^{4'}$	MBP R$^{13'}$-MM	MBP R$^{13'}$-ADM	MBP R$^{13'}$-SDM
				RT loop			
Y91		Y91		Y91	Y91	Y91	Y91
	D92		*D92*	*D92*	*D92*	*D92*	*D92*
Y93	Y93	Y93	Y93	Y93	Y93	Y93	Y93
E94[c]	E94	E94	E94	E94	E94	E94	E94
A95[c]	A95		A95	A95	A95	A95	A95
[R,I]96	R96	R96	R96	R96	R96	R96	R96
T97	T97	T97	T97	T97	T97	T97	T97
E98[c]							
D99[c]	D99	D99	D99	D99	D99	D99	D99
D100	D100	D100	D100	D100	D100	D100	D100
				nSrc loop			
E116	E116	E116	E116	E116	E116	E116	E116
G117					G117		
D118	D118	D118	D118	D118	D118		
W119	W119	W119	W119	W119	W119	W119	W119
				βD + 3_{10} helix			
	Y132	*Y132*	*Y132*	*Y132*	*Y132*	*Y132*	*Y132*
P134	P134	P134	P134	P134		P134	P134
	S135	*S135*	*S135*	*S135*			
N136	N136	N136	N136	N136	N136	N136	N136
Y137	Y137	Y137	Y137	Y137	Y137	Y137	Y137

[a] Analyzed with the tool "FirstGlance in Jmol". The majority of the residues are in common with the canonical Fyn SH3 domain; the exceptions (D92, Y132, and S135) are shown in italic type. In all the complexes, stacking of Trp119 in the SH3 domain binding site with Pro5′ in the peptide is always present. [b] Extrapolated from the PDB structures of Fyn SH3. [c] This group of residues was involved in the interaction only in the complexes where the ligand was the whole protein, i.e., Nef protein from human immunodeficiency virus 1 (PDB entries 1avz and 1efn).

and Methods, but also supported the choice to keep the PPII (T$^{1'}$−P$^{7'}$) backbone torsion angles of the ligand constant in the following simulations (see also Materials and Methods). This choice was in agreement with our CD results on the MBP peptide, which were consistent with an N-terminal stable PPII helix, particularly after phosphorylation.

In Table 2 are summarized the "contact residues" of the SH3 domain with the ligand, analyzed for the best structure obtained from each simulation. The docked energies, and the energy value around which each energy histogram (Figure 5) is centered, are summarized in Table 1.

Docking Simulation **ds1**: *Unmodified Peptide.* Comparison of the results of the two docking simulations performed on the unmodifed MBP peptide, to which either Kollman or Gasteiger partial charges were assigned, showed that they converged to the same best complex conformation, with the same very favorable docked energy (−18.8/−18.6 kcal/mol, respectively, Table 1), slightly better than the one calculated for the MBP−calmodulin interaction (*71*). The dissociation constant (K_d) of MBP with calmodulin has been experimentally measured to be in the micromolar range (*12*, *121*). Generally, the interactions of SH3 domains with proteins containing proline-rich sequences are also weak, with experimentally measured dissociation constants in this range, enabling rapid association and dissociation (*41*); therefore, we can surmise that they are of a similar order of magnitude also for interaction of SH3 domains with MBP.

The PPII helix of the MBP peptide lies in the canonical binding pocket, and the flexible backbone region at the C-terminus is bent close to the SH3 domain surface (Figure 6). Analysis of the contact residues (Table 2**)** showed that the positively charged amino acids in the ligand "canonically" interact with the acidic residues that line the binding pocket. In particular, R$^{13'}$ makes a salt bridge with Asp118 in the n-Src loop and interacts with the residues of the 3_{10} helix; the other arginine, R$^{3'}$, that lies just inside the core motif interacts with the negatively charged residues in the RT loop, making a salt bridge with Asp99. The third positive residue in the MBP peptide, K$^{11'}$, makes a cation−π interaction with Trp119 and interacts also with the 3_{10} helix region. Residue P$^{5'}$ in MBP peptide is stacked with the aromatic ring of Trp119 in the SH3 domain, forming a C−H···π noncanonical hydrogen bond, a characteristic interaction of one of the two SH3 domain hydrophobic binding sites (*81*). The proline residues of the ligand in SH3 complexes are implicated in molecular association, employing these interactions with conserved aromatic residues at the binding site (*123*). Here, P$^{7'}$ also forms a C−H···π interaction with Trp 119 and P$^{5'}$ with Y132, as was similarly found for the Abl tyrosine kinase (*123*). Such aromatic residues (along with Asn136) form canonical and noncanonical (i.e., by means of their CH group) hydrogen bonds with the backbone oxygens of the ligand.

Interestingly, the SH3 domain residue Arg96 is also in contact with the MBP peptide, in particular with P$^{6'}$ and S$^{8'}$, but not by the terminal positively charged side chain of Arg, that, as in almost all the known SH3 domain structures, is turned outward.

Docking Simulation **ds2** *and* **ds3**: *Phosphorylated Peptides.* Docking simulations **ds2** and **ds3** were performed to investigate the effects of three kinds of phosphorylation on the MBP peptide: on residue S$^{8'}$, on residue T$^{4'}$, and on both residues T$^{1'}$ and T$^{4'}$. The best complex conformations resulting from the docking of the three phosphorylated peptides superimposed well with each other and with that of the unmodified peptide. The PPII region of the ligand lies in the same site, and although the C-termini show some differences in their backbone and side-chain torsion angles,

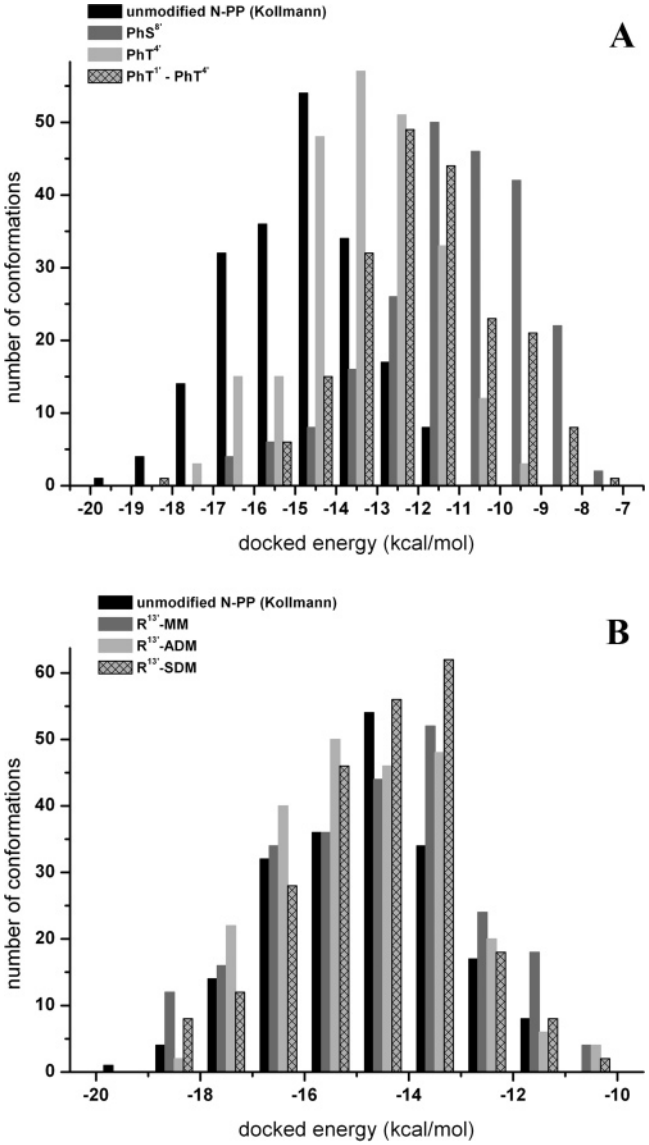

FIGURE 5: Energy histograms of the docking simulations. (A) Energy histogram of the unmodified MBP peptide simulation with the Kollmann partial charges (black bars) is compared with those of $PhS^{8'}$ (dark gray bars), $PhT^{4'}$ (light gray bars), and $PhT^{1'}$-$PhT^{4'}$ (cross-hatched bars). (B) Energy histogram of the unmodified MBP peptide simulation with the Kollman partial charges (black bars) is compared with those of $R^{13'}$-MM (dark gray bars), $R^{13'}$-ADM (light gray bars), and $R^{13'}$-SDM (cross-hatched bars).

they remain oriented in the same direction, forming a bundle of structures occupying the same space (Figure 7).

The contact residues of the peptides in the SH3 domain are listed in Table 2. In comparison with the unmodified peptide, the main preserved interactions in all the complexes are the $R^{3'}$−Asp99 salt bridge, the C−H···π Pro−aromatic interactions (in particular the stacking of $P^{5'}$ with Trp119), and the characteristic H-bonds between the ligand backbone oxygens and the residues Asn136 and Tyr137. The $R^{13'}$ residue maintains the salt bridge with Asp118 in all the complexes except that with the double-phosphorylated peptide, in which it is substituted with a cation−π interaction with Tyr91 and Tyr137 in the RT loop. The $K^{11'}$ residue is the more variable one, changing the orientation of its long side chain from the 3_{10} helix to the RT loop, always forming cation−π interactions with the conserved aromatic residues of the binding site (Trp119, Tyr91, and Tyr137).

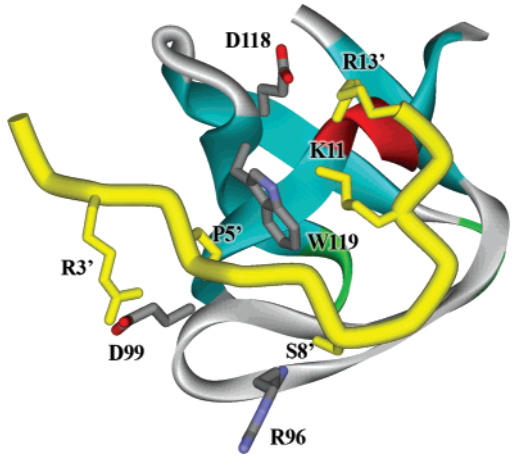

FIGURE 6: Complex of human Fyn SH3 domain with MBP peptide (in yellow) obtained from the **ds1** docking simulation (Kollman partial charges set). The SH3 domain is represented with its secondary structure elements (β-sheets in cyan, 3_{10}-helix in red, and turns in green). The relevant contact residues are shown in stick representation, colored by atom type in the SH3 domain and yellow in the MBP peptide.

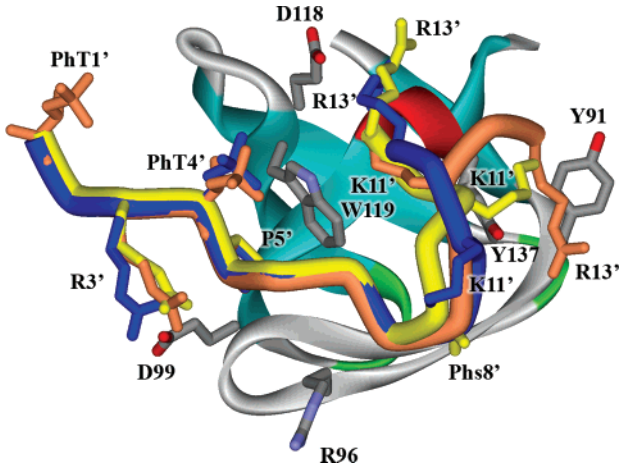

FIGURE 7: Complexes of the human Fyn SH3 domain with the phosphorylated peptides obtained from the docking simulations **ds2** and **ds3**, superimposed for comparison. MBP peptide with posttranslational modification $S^{8'} \rightarrow PhS^{8'}$ is shown in yellow; MBP peptide with posttranslational modification $T^{4'} \rightarrow PhT^{4'}$ alone is shown in blue; and MBP peptide with posttranslational modifications $T^{1'} \rightarrow PhT^{1'} + T^{4'} \rightarrow PhT^{4'}$ is shown in orange. The relevant contact residues are shown in stick representation, colored by atom type in the SH3 domain and by ligand color in the docked peptides.

The $PhS^{8'}$ side chain shows a different orientation compared to the unmodified $S^{8'}$ residue, due to the phosphate steric hindrance, and the complexes of the SH3 domain with the $PhS^{8'}$ peptide (**ds2**) have a greater docked energy (i.e., less favorable) than the unmodified MBP peptide complexes, clearly evaluable from the energy histogram in Figure 5. Residue Arg96 is still in contact with $PhS^{8'}$, but this kind of interaction does not seem to involve the two charged side chains. It is possible that the rigidity (real and built-in) of the PPII backbone segment that flanks the $PhS^{8'}$ residue prevents the modified side chain from better adapting to the receptor surface, enhancing the complex interaction energy.

The docked energies of the complexes of the SH3 domain with the $PhT^{4'}$ peptide (**ds3a**) are also slightly less favorable than for the unmodified MBP peptide (see the energy histograms in Figure 5, as well as Table 1). Although $PhT^{4'}$ might be more restrained because it lies in a more rigid region

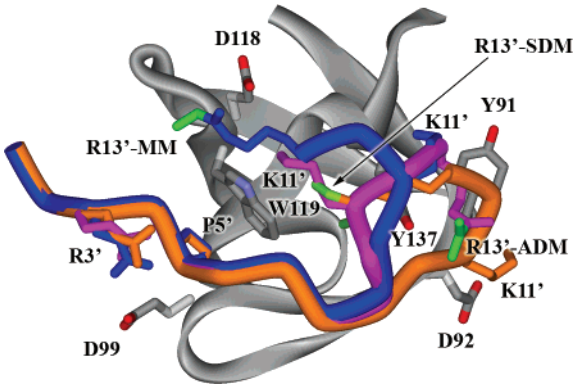

FIGURE 8: Complexes of human Fyn SH3 domain with $R^{13'}$-methylated peptides obtained from docking simulations **ds4**, **ds5**, and **ds6**, superimposed for comparison. MBP peptide with $R^{13'}$-MM is colored dark blue; MBP peptide with $R^{13'}$-ADM is colored magenta; MBP peptide with $R^{13'}$-SDM is colored orange. The methylated atoms are highlighted in green; the relevant contact residues are shown in stick representation, colored by atom type in the SH3 domain and by ligand color in the docked peptides. The cartoon representation of the SH3 domain is totally gray for the sake of clarity.

(real and built-in) of the peptide (center of the PPII backbone) than does $PhS^{8'}$, the absolute docked energy for **ds3a** is more favorable than for **ds2**. Therefore, the less favorable interaction of the $PhS^{8'}$ peptide cannot be explained by backbone flexibility.

The double phosphorylation of the MBP peptide on $T^{1'}$ and $T^{4'}$ increased the docked energies with respect to the single PhT4′ mutation (Figure 5), reaching values comparable to those of the $PhS^{8'}$ peptide.

Docking Simulations **ds4**, **ds5**, *and* **ds6**: *$R^{13'}$-Methylated Peptide.* With the methylation of residue $R^{13'}$, which remained charged, the steric hindrance caused by the mono- or dimethyl (symmetrical and asymmetrical) groups results in the ligand peptide adjusting the position of this long side chain to optimize the interaction and its conformation in the binding site. Thus, the best methylated complexes have good docked energies, of the same magnitude as the unmodified MBP peptide (see Table 1 and Figure 5). Also in this case, the best complexes obtained for the three methylated ligands superimpose very well with each other and with the unmodified one in the PPII region (Figure 8). The stacking of $P^{5'}$ with Trp119 is still present, involving the weak CH$\cdots\pi$ interactions of the prolines with the aromatic residues of the binding site, underlying the importance of pairing these residues for molecular recognition and association. Canonical and noncanonical hydrogen bonds are preserved, in particular with Asn136.

The C-terminus ($G^{10'}-R^{13'}$) shows a larger shift than for the phosphorylated ligands, in order to make more favorable interactions with the $R^{13'}$ methylated residue (Figure 8). In the monomethylated ligand, the $R^{13'}$-MM residue is near the n-Src loop but nevertheless forms a salt bridge with Asp118. Instead, $R^{13'}$-ADM shifts toward the first residues of the RT loop, interacting with the aromatic rings of Tyr91 and Tyr137 by cation$-\pi$ interactions. The posttranslational modification $R^{13'}$-SDM is peculiar to MBP and only a few other proteins. The C-terminal backbone (from $G^{10'}$ to $R^{13'}$-SDM) is affected the most by this modification, being strongly bent to the center of the binding pocket in a way that causes the $R^{13'}$ side chain, with its symmetric methyl groups, to interact with Trp119, making more hydrophobic contacts than polar ones. Nonetheless, a cation$-\pi$ interaction with Tyr137 is still present. Due to the shift of the C-terminus, the charged K11′ also has different orientations (toward the RT loop or the n-Src loop), but always forming salt bridges or cation$-\pi$ interactions.

Considerations about Docking Simulations with Small Peptides. Although computational resources available to us restricted the simulations to modeling a 13-residue MBP peptide alone, this simplification may be insufficient to describe the interaction. The whole protein, especially when membrane-associated, should be able to interact more strongly with the SH3 domain (cf. refs *11*, *13*, and *17*). Moreover, the interaction could involve also other structured regions in addition to the PPII segment, as is the case for the Nef protein (*124*, *125*). This consideration is plausible, as seems to be the case with calmodulin, where the classic MBP isoforms interact strongly but Golli-MBP isoforms (with almost identical predicted calmodulin targets on them) interact weakly (*12*, *88*, *89*, *121*). In addition, posttranslational modifications both locally and distally can modulate the interaction as they do for MBP interacting with calmodulin, actin, and tubulin (*12*, *13*, *15*−*17*, *71*). This effect has been seen here in the altered interaction of quasi-deiminated MBP with SH3 domains on the array (Figure 3); the glutamine-substituted arginines are distributed throughout the protein and are not localized in the proline-rich segment. Similarly, combinatorial phosphorylation at the various possible sites (*46*) may also have a significant effect, as can be seen in the less favorable complex of the double-mutated $PhT^{1'}$-$PhT^{4'}$ peptide. The methylation of R104 may not be important in modulating the interaction with SH3 domains, however. Although the conformation of the MBP peptide in the SH3 domain pocket changed significantly with Arg methylation or with phosphorylation, new interactions were able to substitute for those lost, in order to stabilize the complex. These multiple potential interaction sites on the SH3 domain thus allow an SH3 domain to bind promiscuously to a variety of ligands (*46*). Although we could not compare binding of the entire protein with nonmethylated Arg and methylated Arg, the rmC1 used for array binding has a nonmethylated Arg, whereas the natural bC1 used for binding of the Fyn SH3 domain to lipid vesicles has a methylated Arg. Since both proteins bound the Fyn SH3 domain, this observation suggests that Arg methylation does not have a large effect on binding, in agreement with the peptide simulations. Although R104 methylation in 18.5 kDa MBP is associated with healthy myelin (*5*), its exact biological significance remains unknown.

CONCLUDING REMARKS

Myelin basic protein is a multifunctional protein, based on its variety of splice isoforms and myriad posttranslational modifications and its interactions with membranes and proteins such as calmodulin, actin, and tubulin (*2*, *3*). A central segment representing an immunodominant epitope in multiple sclerosis has been extensively characterized and found to be a membrane-surface-associated amphipathic α-helix (*18*, *90*, *91*). Immediately adjacent to this motif is a proline-rich segment that has previously been noted to contain a potential SH3 ligand (*37*). Here, we have shown by CD spectroscopy that this proline-rich segment of MBP

forms a PPII helix in vitro under physiological conditions and that phosphorylation at a constituent threonyl residue has a stabilizing effect on its conformation.

Previous preliminary experimental investigations have shown that 18.5 kDa MBP interacts with SH3-domain-containing proteins in vitro (*38*), which we have explored here more comprehensively using SH3 domain microarrays. We have shown here that the minimally modified 18.5 kDa recombinant murine MBP isoform rmC1 bound to the SH3 domains of the Src tyrosine kinases Yes1, Fyn, and c-Src, the kinases Abl, Itk, and PSD95, and the actin-binding protein cortactin. Several Src kinases, including Fyn and Src, and cortactin are present in oligodendrocytes and/or myelin (*63*, *126*). PSD95 (presynaptic density protein 95), a membrane-associated guanylate kinase (MAGUK), is not known to be present in oligodendrocytes. However, the tight junction protein ZO-1, also a MAGUK, is present in oligodendrocytes and myelin tight junctions (*127*, *128*), and its SH3 domain has 57% similarity to that of PSD-95 (*129*). We have also demonstrated that the Fyn SH3 domain can bind to membrane-associated MBP. It is known that MBP binds to cytoskeletal proteins (*2*, *3*, *11*, *13*, *15*−*17*) and is required to transmit extracellular signals, provided by anti-GalC antibody, to the oligodendrocyte cytoskeleton (*130*). Binding of MBP to the SH3 domains of several proteins supports a role for MBP in signal transduction and membrane−cytoskeleton associations.

Spin-labeled P93C and S99C, in membrane-associated rmC1 and rmC8, was exposed to the aqueous phase (*90*, *92*), suggesting that the entire Pro-rich region of both isomers should be accessible to enzymes and other proteins, including those with SH3 domains, even when MBP is associated with the membrane. Indeed, when bound to a lipid membrane, MBP was cleaved by trypsin at R94−T95 and R104−G105, although two other tryptic sites closer to the N-terminus, R22−H23 and R62−T63, were protected (*131*). The present results, which show that this region of MBP binds Fyn to the vesicle surface, support the conclusion that the Pro-rich region is accessible on the bilayer surface and suggest that MBP could bind Fyn and other SH3-domain-containing proteins to the oligodendrocyte and/or myelin membrane.

In order to gain further structural insight, we have investigated via molecular docking simulations the interaction of the putative SH3 ligand of classic MBP with an SH3-domain-containing protein. The results suggested that the strength of the interaction would be of the same order of magnitude as with calmodulin (*71*), from which we can hypothesize that the dissociation constants (K_d) are in the same micromolar range. Thus, there would be rapid association and dissociation, an important feature for signaling hubs. Molecular recognition and association could be mediated by the weak CH$\cdots\pi$ interactions of the ligand prolyl residues with the aromatic residues in the binding site, in particular by the stacking of a proline with the tryptophanyl residue in the n-Src loop (here Trp119), that is characteristic of this kind of interaction and was identified in particular for SH3 domain binding (*123*). Lysyl and arginyl residues in the peptide interacted via salt bridges and cation$-\pi$ interactions with negatively charged and aromatic residues in the SH3 domain. Posttranslational modification (phosphorylation or methylation) of the ligand did not cause any major inhibition of the binding beyond a somewhat less favorable interaction, especially for the $S^{8'}$ phosphorylated and $T^{1'}$-$T^{4'}$ double-phosphorylated peptides.

ACKNOWLEDGMENT

We are grateful to Dr. Alan Davidson (Toronto) for the Fyn SH3 domain and to Professor Paolo Cavatorta (Parma) for helpful discussions.

REFERENCES

1. Campagnoni, A. T. and Campagnoni, C. (2004) Myelin basic protein gene, in *Myelin Biology and Disorders* (Lazzarini, R. A., Griffin, J. W., Lassman, H., Nave, K.-A., Miller, R. H., and Trapp, B. D., Eds.) pp 387−400, Elsevier Academic Press, San Diego, CA.
2. Harauz, G., Ishiyama, N., Hill, C. M. D., Bates, I. R., Libich, D. S., and Farès, C. (2004) Myelin basic protein - diverse conformational states of an intrinsically unstructured protein and its roles in myelin assembly and multiple sclerosis, *Micron 35*, 503−542.
3. Boggs, J. M. (2006) Myelin basic protein: a multifunctional protein, *Cell Mol. Life Sci. 63*, 1945−1961.
4. Jacobs, E. C., Pribyl, T. M., Kampf, K., Campagnoni, C., Colwell, C. S., Reyes, S. D., Martin, M., Handley, V., Hiltner, T. D., Readhead, C., Jacobs, R. E., Messing, A., Fisher, R. S., and Campagnoni, A. T. (2005) Region-specific myelin pathology in mice lacking the golli products of the myelin basic protein gene, *J. Neurosci. 25*, 7004−7013.
5. Kim, J. K., Mastronardi, F. G., Wood, D. D., Lubman, D. M., Zand, R., and Moscarello, M. A. (2003) Multiple sclerosis: an important role for post-translational modifications of myelin basic protein in pathogenesis, *Mol. Cell. Proteomics 2*, 453−462.
6. Mastronardi, F. G., and Moscarello, M. A. (2005) Molecules affecting myelin stability: a novel hypothesis regarding the pathogenesis of multiple sclerosis, *J. Neurosci. Res. 80*, 301−308.
7. Harauz, G., and Musse, A. A. (2007) A tale of two citrullines - structural and functional aspects of myelin basic protein deimination in health and disease, *Neurochem. Res. 32*, 137−158.
8. Moscarello, M. A., Mastronardi, F. G., and Wood, D. D. (2007) The role of citrullinated proteins suggests a novel mechanism in the pathogenesis of multiple sclerosis, *Neurochem. Res. 32*, 251−256.
9. Ramwani, J. J., Epand, R. M., and Moscarello, M. A. (1989) Secondary structure of charge isomers of myelin basic protein before and after phosphorylation, *Biochemistry 28*, 6538−6543.
10. Deibler, G. E., Stone, A. L., and Kies, M. W. (1990) Role of phosphorylation in conformational adaptability of bovine myelin basic protein, *Proteins: Struct., Funct., Genet. 7*, 32−40.
11. Boggs, J. M., and Rangaraj, G. (2000) Interaction of lipid-bound myelin basic protein with actin filaments and calmodulin, *Biochemistry 39*, 7799−7806.
12. Libich, D. S., Hill, C. M. D., Bates, I. R., Hallett, F. R., Armstrong, S., Siemiarczuk, A., and Harauz, G. (2003) Interaction of the 18.5-kD isoform of myelin basic protein with Ca^{2+}-calmodulin: effects of deimination assessed by intrinsic Trp fluorescence spectroscopy, dynamic light scattering, and circular dichroism, *Protein Sci. 12*, 1507−1521.
13. Boggs, J. M., Rangaraj, G., Hill, C. M., Bates, I. R., Heng, Y. M., and Harauz, G. (2005) Effect of arginine loss in myelin basic protein, as occurs in its deiminated charge isoform, on mediation of actin polymerization and actin binding to a lipid membrane in vitro, *Biochemistry 44*, 3524−3534.
14. DeBruin, L. S., Haines, J. D., Wellhauser, L. A., Radeva, G., Schonmann, V., Bienzle, D., and Harauz, G. (2005) Developmental partitioning of myelin basic protein into membrane microdomains, *J. Neurosci. Res. 80*, 211−225.
15. Hill, C. M. D., and Harauz, G. (2005) Charge effects modulate actin assembly by classic myelin basic protein isoforms, *Biochem. Biophys. Res. Commun. 329*, 362−369.
16. Hill, C. M. D., Libich, D. S., and Harauz, G. (2005) Assembly of tubulin by classic myelin basic protein isoforms and regulation by post-translational modification, *Biochemistry 44*, 16672−16683.
17. Boggs, J. M., Rangaraj, G., Gao, W., and Heng, Y. M. (2006) Effect of phosphorylation of myelin basic protein by MAPK on

its interactions with actin and actin binding to a lipid membrane in vitro, *Biochemistry 45*, 391−401.
18. Musse, A. A., Boggs, J. M., and Harauz, G. (2006) Deimination of membrane-bound myelin basic protein in multiple sclerosis exposes an immunodominant epitope, *Proc. Natl. Acad. Sci. U.S.A. 103*, 4422−4427.
19. DeBruin, L. S., and Harauz, G. (2007) White matter rafting - membrane microdomains in myelin, *Neurochem. Res. 32*, 213−228.
20. Yang, X. J. (2005) Multisite protein modification and intramolecular signaling, *Oncogene 24*, 1653−1662.
21. Seet, B. T., Dikic, I., Zhou, M. M., and Pawson, T. (2006) Reading protein modifications with interaction domains, *Nat. Rev. Mol. Cell Biol. 7*, 473−483.
22. Uversky, V. N., Gillespie, J. R., and Fink, A. L. (2000) Why are "natively unfolded" proteins unstructured under physiologic conditions?, *Proteins: Struct., Funct., Genet. 41*, 415−427.
23. Dyson, H. J., and Wright, P. E. (2005) Intrinsically unstructured proteins and their functions, *Nat. Rev. Mol. Cell Biol. 6*, 197−208.
24. Tompa, P. (2005) The interplay between structure and function in intrinsically unstructured proteins, *FEBS Lett. 579*, 3346−3354.
25. Receveur-Bréchot, V., Bourhis, J. M., Uversky, V. N., Canard, B., and Longhi, S. (2006) Assessing protein disorder and induced folding, *Proteins: Struct., Funct., Bioinf. 62*, 24−45.
26. Dunker, A. K., Cortese, M. S., Romero, P., Iakoucheva, L. M., and Uversky, V. N. (2005) Flexible nets. The roles of intrinsic disorder in protein interaction networks, *FEBS J. 272*, 5129−5148.
27. Uversky, V. N., Oldfield, C. J., and Dunker, A. K. (2005) Showing your ID: intrinsic disorder as an ID for recognition, regulation and cell signaling, *J. Mol. Recognit. 18*, 343−384.
28. Haynes, C., Oldfield, C. J., Ji, F., Klitgord, N., Cusick, M. E., Radivojac, P., Uversky, V. N., Vidal, M., and Iakoucheva, L. M. (2006) Intrinsic disorder is a common feature of hub proteins from four eukaryotic interactomes, *PLoS Comput. Biol. 2*, e100.
29. Iakoucheva, L. M., Radivojac, P., Brown, C. J., O'Connor, T. R., Sikes, J. G., Obradovic, Z., and Dunker, A. K. (2004) The importance of intrinsic disorder for protein phosphorylation, *Nucleic Acids Res. 32*, 1037−1049.
30. Serber, Z., and Ferrell, J. E., Jr. (2007) Tuning bulk electrostatics to regulate protein function, *Cell 128*, 441−444.
31. Dyer, C. A., Phillbotte, T., Wolf, M. K., and Billings-Gagliardi, S. (1997) Regulation of cytoskeleton by myelin components: studies on shiverer oligodendrocytes carrying an *Mbp* transgene, *Dev. Neurosci. 19*, 395−409.
32. Dyer, C. A. (2002) The structure and function of myelin: from inert membrane to perfusion pump, *Neurochem. Res. 27*, 1279−1292.
33. Fitzner, D., Schneider, A., Kippert, A., Mobius, W., Willig, K. I., Hell, S. W., Bunt, G., Gaus, K., and Simons, M. (2006) Myelin basic protein-dependent plasma membrane reorganization in the formation of myelin, *EMBO J. 25*, 5037−5048.
34. Harauz, G., Ishiyama, N., and Bates, I. R. (2000) Analogous structural motifs in myelin basic protein and in MARCKS, *Mol. Cell. Biochem. 209*, 155−163.
35. Lee, G. (2005) Tau and src family tyrosine kinases, *Biochim. Biophys. Acta 1739*, 323−330.
36. Csizmok, V., Bokor, M., Banki, P., Klement, E., Medzihradszky, K. F., Friedrich, P., Tompa, K., and Tompa, P. (2005) Primary contact sites in intrinsically unstructured proteins: the case of calpastatin and microtubule-associated protein 2, *Biochemistry 44*, 3955−3964.
37. Moscarello, M. A. (1997) Myelin basic protein, the "executive" molecule of the myelin membrane, in *Cell Biology and Pathology of Myelin: Evolving Biological Concepts and Therapeutic Approaches.* (Juurlink, B. H. J., Devon, R. M., Doucette, J. R., Nazarali, A. J., Schreyer, D. J., and Verge, V. M. K., Eds.) pp 13−25, Plenum Press, New York.
38. DeBruin, L. S., Wood, D. D., Moscarello, M. A., and Harauz, G. (2002) Interactions of myelin basic protein with SH3-domain containing proteins, International Society of Neurochemistry Small Conference, and European Science Foundation Exploratory Workshop on Myelin Structure and its Role in Autoimmunity, Potenza, Italy.
39. Musacchio, A., Gibson, T., Lehto, V. P., and Saraste, M. (1992) SH3 - an abundant protein domain in search of a function, *FEBS Lett. 307*, 55−61.
40. Dalgarno, D. C., Botfield, M. C., and Rickles, R. J. (1997) SH3 domains and drug design: ligands, structure, and biological function, *Biopolymers 43*, 383−400.
41. Mayer, B. J. (2001) SH3 domains: complexity in moderation, *J. Cell Sci. 114*, 1253−1263.
42. Macias, M. J., Wiesner, S., and Sudol, M. (2002) WW and SH3 domains, two different scaffolds to recognize proline-rich ligands, *FEBS Lett. 513*, 30−37.
43. Boggon, T. J., and Eck, M. J. (2004) Structure and regulation of Src family kinases, *Oncogene 23*, 7918−7927.
44. Roskoski, R., Jr. (2004) Src protein-tyrosine kinase structure and regulation, *Biochem. Biophys. Res. Commun. 324*, 1155−1164.
45. Beltrao, P., and Serrano, L. (2005) Comparative genomics and disorder prediction identify biologically relevant SH3 protein interactions, *PLoS Comput. Biol. 1*, e26.
46. Li, S. S. (2005) Specificity and versatility of SH3 and other proline-recognition domains: structural basis and implications for cellular signal transduction, *Biochem. J. 390*, 641−653.
47. Kami, K., Takeya, R., Sumimoto, H., and Kohda, D. (2002) Diverse recognition of non-PxxP peptide ligands by the SH3 domains from p67(phox), Grb2 and Pex13p, *EMBO J. 21*, 4268−4276.
48. Fazi, B., Cope, M. J., Douangamath, A., Ferracuti, S., Schirwitz, K., Zucconi, A., Drubin, D. G., Wilmanns, M., Cesareni, G., and Castagnoli, L. (2002) Unusual binding properties of the SH3 domain of the yeast actin-binding protein Abp1: structural and functional analysis, *J. Biol. Chem. 277*, 5290−5298.
49. Liu, Q., Berry, D., Nash, P., Pawson, T., McGlade, C. J., and Li, S. S. (2003) Structural basis for specific binding of the Gads SH3 domain to an RxxK motif-containing SLP-76 peptide: a novel mode of peptide recognition, *Mol. Cell 11*, 471−481.
50. Jia, C. Y., Nie, J., Wu, C., Li, C., and Li, S. S. (2005) Novel Src homology 3 domain-binding motifs identified from proteomic screen of a Pro-rich region, *Mol. Cell. Proteomics 4*, 1155−1166.
51. Hofmann, G., Schweimer, K., Kiessling, A., Hofinger, E., Bauer, F., Hoffmann, S., Rosch, P., Campbell, I. D., Werner, J. M., and Sticht, H. (2005) Binding, domain orientation, and dynamics of the Lck SH3-SH2 domain pair and comparison with other Src-family kinases, *Biochemistry 44*, 13043−13050.
52. Bauer, F., Schweimer, K., Meiselbach, H., Hoffmann, S., Rosch, P., and Sticht, H. (2005) Structural characterization of Lyn-SH3 domain in complex with a herpesviral protein reveals an extended recognition motif that enhances binding affinity, *Protein Sci. 14*, 2487−2498.
53. Liu, J., Li, M., Ran, X., Fan, J. S., and Song, J. (2006) Structural insight into the binding diversity between the human Nck2 SH3 domains and proline-rich proteins, *Biochemistry 45*, 7171−7184.
54. Moncalian, G., Cardenes, N., Deribe, Y. L., Spinola-Amilibia, M., Dikic, I., and Bravo, J. (2006) Atypical polyproline recognition by the CMS N-terminal Src homology 3 domain, *J. Biol. Chem. 281*, 38845−38853.
55. Schmidt, H., Hoffmann, S., Tran, T., Stoldt, M., Stangler, T., Wiesehan, K., and Willbold, D. (2007) Solution structure of a Hck SH3 domain ligand complex reveals novel interaction modes, *J. Mol. Biol. 365*, 1517−1532.
56. Williamson, M. P. (1994) The structure and function of proline-rich regions in proteins, *Biochem. J. 297* (Pt. 2), 249−260.
57. Kay, B. K., Williamson, M. P., and Sudol, M. (2000) The importance of being proline: the interaction of proline-rich motifs in signaling proteins with their cognate domains, *FASEB J. 14*, 231−241.
58. Rath, A., Davidson, A. R., and Deber, C. M. (2005) The structure of "unstructured" regions in peptides and proteins: role of the polyproline II helix in protein folding and recognition, *Biopolymers 80*, 179−185.
59. Umemori, H., Sato, S., Yagi, T., Aizawa, S., and Yamamoto, T. (1994) Initial events of myelination involve Fyn tyrosine kinase signalling, *Nature 367*, 572−576.
60. Umemori, H., Kadowaki, Y., Hirosawa, K., Yoshida, Y., Hironaka, K., Okano, H., and Yamamoto, T. (1999) Stimulation of myelin basic protein gene transcription by Fyn tyrosine kinase for myelination, *J. Neurosci. 19*, 1393−1397.
61. Osterhout, D. J., Wolven, A., Wolf, R. M., Resh, M. D., and Chao, M. V. (1999) Morphological differentiation of oligodendrocytes requires activation of Fyn tyrosine kinase, *J. Cell Biol. 145*, 1209−1218.

62. Seiwa, C., Sugiyama, I., Yagi, T., Iguchi, T., and Asou, H. (2000) Fyn tyrosine kinase participates in the compact myelin sheath formation in the central nervous system, *Neurosci. Res. 37*, 21−31.
63. Sperber, B. R., Boyle-Walsh, E. A., Engleka, M. J., Gadue, P., Peterson, A. C., Stein, P. L., Scherer, S. S., and McMorris, F. A. (2001) A unique role for Fyn in CNS myelination, *J. Neurosci. 21*, 2039−2047.
64. Seiwa, C., Yamamoto, M., Tanaka, K., Fukutake, M., Ueki, T., Takeda, S., Sakai, R., Ishige, A., Watanabe, K., Akita, M., Yagi, T., Tanaka, K., and Asou, H. (2007) Restoration of FcRgamma/Fyn signaling repairs central nervous system demyelination, *J. Neurosci. Res. 85*, 954−966.
65. Krämer, E. M., Klein, C., Koch, T., Boytinck, M., and Trotter, J. (1999) Compartmentation of Fyn kinase with glycosylphosphatidylinositol-anchored molecules in oligodendrocytes facilitates kinase activation during myelination, *J. Biol. Chem. 274*, 29042−29049.
66. DeBruin, L. S., Haines, J. D., Bienzle, D., and Harauz, G. (2006) Partitioning of myelin basic protein into membrane microdomains in a spontaneously demyelinating mouse model for multiple sclerosis, *Biochem. Cell Biol. 84*, 993−1005.
67. Noble, M. E., Musacchio, A., Saraste, M., Courtneidge, S. A., and Wierenga, R. K. (1993) Crystal structure of the SH3 domain in human Fyn; comparison of the three-dimensional structures of SH3 domains in tyrosine kinases and spectrin, *EMBO J. 12*, 2617−2624.
68. Musacchio, A., Saraste, M., and Wilmanns, M. (1994) High-resolution crystal structures of tyrosine kinase SH3 domains complexed with proline-rich peptides, *Nat. Struct. Biol. 1*, 546−551.
69. Yu, H., Chen, J. K., Feng, S., Dalgarno, D. C., Brauer, A. W., and Schreiber, S. L. (1994) Structural basis for the binding of proline-rich peptides to SH3 domains, *Cell 76*, 933−945.
70. Renzoni, D. A., Pugh, D. J., Siligardi, G., Das, P., Morton, C. J., Rossi, C., Waterfield, M. D., Campbell, I. D., and Ladbury, J. E. (1996) Structural and thermodynamic characterization of the interaction of the SH3 domain from Fyn with the proline-rich binding site on the p85 subunit of PI3-kinase, *Biochemistry 35*, 15646−15653.
71. Polverini, E., Boggs, J. M., Bates, I. R., Harauz, G., and Cavatorta, P. (2004) Electron paramagnetic resonance spectroscopy and molecular modelling of the interaction of myelin basic protein (MBP) with calmodulin (CaM)-diversity and conformational adaptability of MBP CaM-targets, *J. Struct. Biol. 148*, 353−369.
72. Sherman, F., Stewart, J. W., and Tsunasawa, S. (1985) Methionine or not methionine at the beginning of a protein, *Bioessays 3*, 27−31.
73. Bates, I. R., Matharu, P., Ishiyama, N., Rochon, D., Wood, D. D., Polverini, E., Moscarello, M. A., Viner, N. J., and Harauz, G. (2000) Characterization of a recombinant murine 18.5-kDa myelin basic protein, *Protein Expression Purif. 20*, 285−299.
74. Cheifetz, S., Moscarello, M. A., and Deber, C. M. (1984) NMR investigation of the charge isomers of bovine myelin basic protein, *Arch. Biochem. Biophys. 233*, 151−160.
75. Bates, I. R., Libich, D. S., Wood, D. D., Moscarello, M. A., and Harauz, G. (2002) An Arg/Lys → Gln mutant of recombinant murine myelin basic protein as a mimic of the deiminated form implicated in multiple sclerosis, *Protein Expression Purif. 25*, 330−341.
76. Maxwell, K. L., and Davidson, A. R. (1998) Mutagenesis of a buried polar interaction in an SH3 domain: sequence conservation provides the best prediction of stability effects, *Biochemistry 37*, 16172−16182.
77. Peterson, G. L. (1977) A simplification of the protein assay method of Lowry et al. which is more generally applicable, *Anal. Biochem. 83*, 346−356.
78. Molnar, L., Vago, I., and Feher, A. (2003) Construction of a Linux based chemical and biological information system, *Mol. Diversity 7*, 61−67.
79. Clark, M., Cramer, R. D., and Vanopdenbosch, N. (1989) Validation of the general-purpose Tripos 5.2 force-field, *J. Comput. Chem. 10*, 982−1012.
80. Berman, H. M., Westbrook, J., Feng, Z., Gilliland, G., Bhat, T. N., Weissig, H., Shindyalov, I. N., and Bourne, P. E. (2000) The Protein Data Bank, *Nucleic Acids Res. 28*, 235−242.
81. Cesareni, G., Panni, S., Nardelli, G., and Castagnoli, L. (2002) Can we infer peptide recognition specificity mediated by SH3 domains?, *FEBS Lett. 513*, 38−44.
82. Weiner, S. J., Kollman, P. A., Case, D. A., Chandra-Singh, U., Ghio, C., Alagona, G., Profeta, S., Jr., and Weiner, P. (1984) A new force field for molecular mechanical stimulation of nucleic acids and proteins, *J. Am. Chem. Soc. 106*, 765−784.
83. Gasteiger, J., and Marsili, M. (1980) Iterative partial equalisation of orbital electronegativity - a rapid access to atomic charges, *Tetrahedron 36*, 3219−3228.
84. Morris, G. M., Goodsell, D. S., Halliday, R. S., Huey, R., Hart, W. E., Below, R. K., and Olson, A. J. (1998) Automated docking using a Lamarckian genetic algorithm and an empirical binding free energy function, *J. Comput. Chem. 19*, 1639−1662.
85. Guex, N., and Peitsch, M. C. (1997) SWISS-MODEL and the Swiss-PdbViewer: an environment for comparative protein modeling, *Electrophoresis 18*, 2714−2723.
86. Sayle, R. A. and Milner-White, E. J. (1995) RASMOL: biomolecular graphics for all, *Trends Biochem. Sci. 20*, 374.
87. Babu, M. M. (2003) NCI: A server to identify non-canonical interactions in protein structures, *Nucleic Acids Res. 31*, 3345−3348.
88. Kaur, J., Libich, D. S., Campagnoni, C. W., Wood, D. D., Moscarello, M. A., Campagnoni, A. T., and Harauz, G. (2003) Expression and properties of the recombinant murine Golli-myelin basic protein isoform J37, *J. Neurosci. Res. 71*, 777−784.
89. Bamm, V. V., Ahmed, M. A., Ladizhansky, V., and Harauz, G. (2007) Purification and spectroscopic characterization of the recombinant BG21 isoform of murine golli myelin basic protein, *J. Neurosci. Res. 85*, 272−284.
90. Bates, I. R., Feix, J. B., Boggs, J. M., and Harauz, G. (2004) An immunodominant epitope of myelin basic protein is an amphipathic alpha-helix, *J. Biol. Chem. 279*, 5757−5764.
91. Farès, C., Libich, D. S., and Harauz, G. (2006) Solution NMR structure of an immunodominant epitope of myelin basic protein. Conformational dependence on environment of an intrinsically unstructured protein, *FEBS J. 273*, 601−614.
92. Bates, I. R., Boggs, J. M., Feix, J. B., and Harauz, G. (2003) Membrane-anchoring and charge effects in the interaction of myelin basic protein with lipid bilayers studied by site-directed spin labeling, *J. Biol. Chem. 278*, 29041−29047.
93. Hirschberg, D., Radmark, O., Jornvall, H., and Bergman, T. (2003) Thr94 in bovine myelin basic protein is a second phosphorylation site for 42-kDa mitogen-activated protein kinase (ERK2), *J. Protein Chem. 22*, 177−181.
94. Erickson, A. K., Payne, D. M., Martino, P. A., Rossomando, A. J., Shabanowitz, J., Weber, M. J., Hunt, D. F., and Sturgill, T. W. (1990) Identification by mass spectrometry of threonine 97 in bovine myelin basic protein as a specific phosphorylation site for mitogen-activated protein kinase, *J. Biol. Chem. 265*, 19728−19735.
95. Yu, J. S., and Yang, S. D. (1994) Protein kinase FA/glycogen synthase kinase-3 predominantly phosphorylates the in vivo site Thr97-Pro in brain myelin basic protein: evidence for Thr-Pro and Ser-Arg-X-X-Ser as consensus sequence motifs, *J. Neurochem. 62*, 1596−1603.
96. Bedford, M. T., Frankel, A., Yaffe, M. B., Clarke, S., Leder, P., and Richard, S. (2000) Arginine methylation inhibits the binding of proline-rich ligands to Src homology 3, but not WW, domains, *J. Biol. Chem. 275*, 16030−16036.
97. Bedford, M. T., and Richard, S. (2005) Arginine methylation: an emerging regulator of protein function, *Mol. Cell 18*, 263−272.
98. Boisvert, F. M., Chenard, C. A., and Richard, S. (2005) Protein interfaces in signaling regulated by arginine methylation, *Sci. STKE 2005*, re2.
99. Ostareck-Lederer, A., Ostareck, D. H., Rucknagel, K. P., Schierhorn, A., Moritz, B., Huttelmaier, S., Flach, N., Handoko, L., and Wahle, E. (2006) Asymmetric arginine dimethylation of heterogeneous nuclear ribonucleoprotein K by protein-arginine methyltransferase 1 inhibits its interaction with c-Src, *J. Biol. Chem. 281*, 11115−11125.
100. Raijmakers, R., Zendman, A. J., Egberts, W. V., Vossenaar, E. R., Raats, J., Soede-Huijbregts, C., Rutjes, F. P., van Veelen, P. A., Drijfhout, J. W., and Pruijn, G. J. (2007) Methylation of arginine residues interferes with citrullination by peptidylarginine deiminases *in vitro*, *J. Mol. Biol. 367*, 1118−1129.
101. Bhaskar, K., Yen, S. H., and Lee, G. (2005) Disease related modifications in tau affect the interaction between Fyn and tau, *J. Biol. Chem. 280*, 35119−35125.
102. Sánchez, C., Tompa, P., Szucs, K., Friedrich, P., and Avila, J. (1996) Phosphorylation and dephosphorylation in the proline-rich

C-terminal domain of microtubule-associated protein 2, *Eur. J. Biochem. 241*, 765−771.
103. Shi, Z., Chen, K., Liu, Z., Sosnick, T. R., and Kallenbach, N. R. (2006) PII structure in the model peptides for unfolded proteins: studies on ubiquitin fragments and several alanine-rich peptides containing QQQ, SSS, FFF, and VVV, *Proteins: Struct., Funct., Bioinf. 63*, 312−321.
104. Whittington, S. J., Chellgren, B. W., Hermann, V. M., and Creamer, T. P. (2005) Urea promotes polyproline II helix formation: implications for protein denatured states, *Biochemistry 44*, 6269−6275.
105. Makowska, J., Rodziewicz-Motowidlo, S., Baginska, K., Vila, J. A., Liwo, A., Chmurzynski, L., and Scheraga, H. A. (2006) Polyproline II conformation is one of many local conformational states and is not an overall conformation of unfolded peptides and proteins, *Proc. Natl. Acad. Sci. U.S.A. 103*, 1744−1749.
106. Chellgren, B. W., and Creamer, T. P. (2004) Short sequences of non-proline residues can adopt the polyproline II helical conformation, *Biochemistry 43*, 5864−5869.
107. Rucker, A. L., and Creamer, T. P. (2002) Polyproline II helical structure in protein unfolded states: lysine peptides revisited, *Protein Sci. 11*, 980−985.
108. Bochicchio, B., and Tamburro, A. M. (2002) Polyproline II structure in proteins: Identification by chiroptical spectroscopies, stability, and functions, *Chirality 14*, 782−792.
109. Shi, Z., Woody, R. W., and Kallenbach, N. R. (2002) Is polyproline II a major backbone conformation in unfolded proteins?, *Adv. Protein Chem. 62*, 163−240.
110. Shi, Z., Olson, C. A., Rose, G. D., Baldwin, R. L., and Kallenbach, N. R. (2002) Polyproline II structure in a sequence of seven alanine residues, *Proc. Natl. Acad. Sci. U.S.A. 99*, 9190−9195.
111. Tholey, A., Lindemann, A., Kinzel, V., and Reed, J. (1999) Direct effects of phosphorylation on the preferred backbone conformation of peptides: a nuclear magnetic resonance study, *Biophys. J. 76*, 76−87.
112. Yang, S. T., Jeon, J. H., Kim, Y., Shin, S. Y., Hahm, K. S., and Kim, J. I. (2006) Possible role of a PXXP central hinge in the antibacterial activity and membrane interaction of PMAP-23, a member of cathelicidin family, *Biochemistry 45*, 1775−1784.
113. Nygaard, E., Mendz, G. L., Moore, W. J., and Martenson, R. E. (1984) NMR of a peptic peptide spanning the triprolyl sequence in myelin basic protein, *Biochemistry 23*, 4003−4010.
114. Fraser, P. E., and Deber, C. M. (1985) Structure and function of the proline-rich region of myelin basic protein, *Biochemistry 24*, 4593−4598.
115. Wulf, G., Finn, G., Suizu, F., and Lu, K. P. (2005) Phosphorylation-specific prolyl isomerization: is there an underlying theme?, *Nat. Cell Biol. 7*, 435−441.
116. Andrew, C. D., Warwicker, J., Jones, G. R., and Doig, A. J. (2002) Effect of phosphorylation on α-helix stability as a function of position, *Biochemistry 41*, 1897−1905.
117. Lu, P. J., Wulf, G., Zhou, X. Z., Davies, P., and Lu, K. P. (1999) The prolyl isomerase Pin1 restores the function of Alzheimer-associated phosphorylated tau protein, *Nature 399*, 784−788.
118. Lu, P. J., Zhou, X. Z., Liou, Y. C., Noel, J. P., and Lu, K. P. (2002) Critical role of WW domain phosphorylation in regulating phosphoserine binding activity and Pin1 function, *J. Biol. Chem. 277*, 2381−2384.
119. Liou, Y. C., Sun, A., Ryo, A., Zhou, X. Z., Yu, Z. X., Huang, H. K., Uchida, T., Bronson, R., Bing, G., Li, X., Hunter, T., and Lu, K. P. (2003) Role of the prolyl isomerase Pin1 in protecting against age-dependent neurodegeneration, *Nature 424*, 556−561.
120. Seet, B. T., Berry, D. M., Maltzman, J. S., Shabason, J., Raina, M., Koretzky, G. A., McGlade, C. J., and Pawson, T. (2007) Efficient T-cell receptor signaling requires a high-affinity interaction between the Gads C-SH3 domain and the SLP-76 RxxK motif, *EMBO J. 26*, 678−689.
121. Libich, D. S., Hill, C. M. D., Haines, J. D., and Harauz, G. (2003) Myelin basic protein has multiple calmodulin-binding sites, *Biochem. Biophys. Res. Commun. 308*, 313−319.
122. Zhou, H. X. (2006) Quantitative relation between intermolecular and intramolecular binding of Pro-rich peptides to SH3 domains, *Biophys. J. 91*, 3170−3181.
123. Bhattacharyya, R., and Chakrabarti, P. (2003) Stereospecific interactions of proline residues in protein structures and complexes, *J. Mol. Biol. 331*, 925−940.
124. Lee, C. H., Saksela, K., Mirza, U. A., Chait, B. T., and Kuriyan, J. (1996) Crystal structure of the conserved core of HIV-1 Nef complexed with a Src family SH3 domain, *Cell 85*, 931−942.
125. Arold, S., Franken, P., Strub, M. P., Hoh, F., Benichou, S., Benarous, R., and Dumas, C. (1997) The crystal structure of HIV-1 Nef protein bound to the Fyn kinase SH3 domain suggests a role for this complex in altered T cell receptor signaling, *Structure 5*, 1361−1372.
126. Kim, H. J., DiBernardo, A. B., Sloane, J. A., Rasband, M. N., Solomon, D., Kosaras, B., Kwak, S. P., and Vartanian, T. K. (2006) WAVE1 is required for oligodendrocyte morphogenesis and normal CNS myelination, *J. Neurosci. 26*, 5849−5859.
127. Morita, K., Sasaki, H., Fujimoto, K., Furuse, M., and Tsukita, S. (1999) Claudin-11/OSP-based tight junctions of myelin sheaths in brain and Sertoli cells in testis, *J. Cell Biol. 145*, 579−588.
128. Li, X., Ionescu, A. V., Lynn, B. D., Lu, S., Kamasawa, N., Morita, M., Davidson, K. G., Yasumura, T., Rash, J. E., and Nagy, J. I. (2004) Connexin47, connexin29 and connexin32 co-expression in oligodendrocytes and Cx47 association with zonula occludens-1 (ZO-1) in mouse brain, *Neuroscience 126*, 611−630.
129. Willott, E., Balda, M. S., Fanning, A. S., Jameson, B., Van Itallie, C., and Anderson, J. M. (1993) The tight junction protein ZO-1 is homologous to the *Drosophila* discs-large tumor suppressor protein of septate junctions, *Proc. Natl. Acad. Sci. U.S.A. 90*, 7834−7838.
130. Dyer, C. A., Philibotte, T. M., Wolf, M. K., and Billings-Gagliardi, S. (1994) Myelin basic protein mediates extracellular signals that regulate microtubule stability in oligodendrocyte membrane sheets, *J. Neurosci. Res. 39*, 97−107.
131. Medveczky, P., Antal, J., Patthy, A., Kekesi, K., Juhasz, G., Szilagyi, L., and Graf, L. (2006) Myelin basic protein, an autoantigen in multiple sclerosis, is selectively processed by human trypsin 4, *FEBS Lett. 580*, 545−552.

BI701336N